Publications of the Astronomical Society of Australia (2025), **42**, e006, 29 pages
doi:10.1017/pasa.2024.115

CAMBRIDGE UNIVERSITY PRESS

Research Article

Investigation on the short-period eclipsing Am binary V404 Aur and GWGem

Xiao-Man Tian[1], Zhi-Hua Wang[2], Li-Ying Zhu[3,4,5] and Jing-Jing Wang[6]

[1]School of Aeronautics, Shandong Jiaotong University, Jinan, China, [2]School of Mathematics and Information Sciences, Yantai University, Yantai, China, [3]Yunnan Observatories, Chinese Academy of Sciences (CAS), Kunming, China, [4]University of the Chinese Academy of Science, Beijing, China, [5]Key Laboratory of the Structure and Evolution of Celestial Objects, Chinese Academy of Sciences, Kunming, China and [6]China University of Petroleum-Beijing at Karamay, Karamay, China

Abstract

The multi-colour complete light curves and low-resolution spectra of two short period eclipsing Am binaries V404 Aur and GW Gem are presented. The stellar atmospheric parameters of the primary stars were derived through the spectra fitting. The observed and TESS-based light curves of them were analysed by using the Wilson-Devinney code. The photometric solutions suggest that both V404 Aur and GW Gem are semi-detached systems with the secondary component filling its critical Roche Lobe, while the former should be a marginal contact binary. The $O-C$ analysis found that the period of V404 Aur is decreasing at a rate of $dP/dt = -1.06(\pm 0.01) \times 10^{-7}$ d yr^{-1}, while the period of GW Gem is increasing at $dP/dt = +2.41(\pm 0.01) \times 10^{-8}$d yr^{-1}. The period decrease of V404 Aur may mainly be caused by the combined effects of the angular momentum loss (AML) via an enhanced stellar wind of the more evolved secondary star and mass transfer between two components. The period increase of GW Gem supports the mass transfer from the secondary to the primary. Both targets may be in the broken contact stage predicted by the thermal relaxation oscillations theory and will eventually evolve to the contact stage. We have collected about 54 well-known eclipsing Am binaries with absolute parameters from the literature. The relations of these parameters are summarised. There are some components that have a higher degree of evolution. The majority of their hydrogen shell may have been stripped away and the stellar internal layer exposed. The accretion processes from such evolved components may be very important for the formation of Am peculiarity in binaries.

Keywords: Stars: binaries: close; stars: binaries: eclipsing; stars: chemically peculiar; stars: binaries: individual (V404 Aur); stars: binaries: individual (GW Gem) stars: evolution

(Received 8 April 2024; revised 23 August 2024; accepted 8 November 2024)

1. Introduction

Metallic-line A-type stars (i.e. Am stars) are CP stars of type A or early F type stars, which show an overabundance of heavy elements (iron-group elements, the rare earth elements) (Conti 1970) and an underabundance of calcium and scandium. The spectra will exhibit the following characteristics: weaker Ca II, K line (Titus & Morgan 1940; Roman, Morgan, & Eggen 1948), but enhanced Sr II line; the scandium and calcium elements are under-abundant while the iron-group elements, Y, Ba, and the rare earth elements are over-abundant (Conti 1970). Next to a weak Ca II K line, Am stars also have weak Ca I 4 226 Å lines. There is a noticeable weakening of the absorption lines in the 4 395–4 400 Å region, which contain significant contributions from Sc II. The weak Ca II K lines and pronounced metallic-line spectra in these objects indicate a discrepancy between the spectral types derived from the strength of the Ca II K line (Sp(K)) and the metallic lines (Sp(m)) of at least five spectral subclasses by definition. While stars with a spectral type difference ($\Delta = Sp(K) - Sp(m)$) of $1 \leq \Delta < 5$ are often referred to as 'marginal Am' (or Am:) stars. Almost all Am stars (more than 90%) are the components of binaries (Abt 1961, 1965; Hubrig et al. 2010). It is generally accepted that the largest equatorial rotational velocity of Am stars is about 120 km s^{-1} (Abt & Moyd 1973; Abt 2000). There is a lack of very short periods of $P_{orb} < 1.2$ days in Am type binaries (Budaj 1996), and the general explanation is that synchronism in such systems would force the primary to rotate faster than 120 km s^{-1}. Nevertheless, Am peculiarity may have no significant correlation with rotational velocity (Monier & Richard 2004; Monier 2005). Many Am stars show anomalous luminosity effect, i.e. the luminosity criteria in certain spectral regions will indicate that the target should be a giant or even supergiant star, whereas in other regions the luminosity will indicate it as a dwarf or even lower luminosity star. The common existence of Am stars in binaries is very noticeable around the chemically peculiar stars; almost all Am stars (more than 90%) are the components of binaries (Abt 1961, 1965; Hubrig et al. 2010). An eclipsing binary containing one or two Am stars is called an eclipsing Am binary. Eclipsing Am binaries are extremely useful and important in investigating the properties of Am stars.

In our earlier work, about 21 600 Am candidates and 754 eclipsing Am binaries were detected based on the low-resolution spectra of the Large Sky Area Multi–Object Fiber Spectroscopic Telescope (LAMOST) (Tian et al. 2023). Some eclipsing Am binary candidates with a short period of less than 1 day were identified, which present challenges to the slow rotation of stars

Corresponding author: Xiao-Man Tian; Email: txmjlx2018@163.com

Cite this article: Tian X-M, Wang Z-H, Zhu L-Y and Wang J-J. (2025) Investigation on the short-period eclipsing Am binary V404 Aur and GWGem. *Publications of the Astronomical Society of Australia* **42**, e006, 1–29. https://doi.org/10.1017/pasa.2024.115

Table 1. Information of V404 Aur, GW Gem and the corresponding comparison and check stars.

Targets	Name	α_{2000}	δ_{2000}	Mag
Variable (V)	V404 Aur	$05^h57^m13^s.51$	$+43°28'16''.76$	$V = 12.74$
Comparison (C)	TYC 2924-2022-1	$05^h57^m30^s.45$	$+43°24'34''.53$	$V = 12.35$
Check (Ch)	TYC 2924-1540-1	$05^h57^m24^s.11$	$+43°32'50''.90$	$V = 11.88$
Variable (V)	GW Gem	$07^h52^m28^s.97$	$+27°09'15''.61$	$V = 10.54$ or $J = 9.826$
Comparison1 (C1)	TYC 1933-570-1	$07^h52^m37^s.48$	$+27°07'45''.85$	$V = 11.10$ or $J = 9.452$
Comparison2 (C2)	2MASS J07521442+2705257	$07^h52^m14^s.42$	$+27°05'25''.71$	$J = 11.583$
Check (Ch)	2MASS J07521241+2703288	$07^h52^m12^s.41$	$+27°03'28''.81$	$J = 10.681$

classified as type Am observed in the previous research. These candidates are significant targets and provide a great opportunity to explore the real relationship between Am–type stars' peculiarity and slow stellar rotation. We have selected some short-period eclipsing Am stars to observe and study. This study focuses on the short-period eclipsing Am binaries V404 Aur and GW Gem.

V404 Aur (NSV 2733, GSC 02924-01750, TYC 2924-1750-1) is an EB type eclipsing Am binary with a period of 0.7543173 d (Samus' et al. 2017). The spectral type of the primary component is kA2hA4mA6 (Tian et al. 2023). No detailed investigation has been carried out on this target.

GW Gem (BD+27 1494, GSC 01933-00692, TYC 1933-692-1) was confirmed as an Algol-type variable star, the period is 0.659444013 d. The spectral type of primary component is kA4hF0mF0 (Tian et al. 2023). The first BV band light curves were observed by Broglia & Conconi (1981). Lee et al. (2009) compiled the four bands light curves which show an inverse O'Connell effect, and the period was found a continuous period increase at a rate of $+(4.2 \pm 0.4) \times 10^{-8}$ d yr^{-1}, corresponding to a fractional period change of $+(1.2 \pm 0.1) \times 10^{-10}$. They concluded that GW Gem is a semidetached system with the secondary star filling its inner Roche Lobe (RL). The mass ratio of GW Gem was around 0.40 (0.46 by Lee et al. 2009 and 0.343 by Yang & Wei 2011).

In this study, the multi-colour high-precision light curves, low-resolution spectrum and $O - C$ diagram with long time spanning eclipse timings were obtained for the short-period eclipsing Am binaries V404 Aur and GW Gem. More accurate geometric and physical parameters were obtained in this study. Meanwhile, the physical parameters of the well-known eclipsing Am binaries were collected. The correlations between the parameters were also been analysed and discussed.

2. Observation and Data Reduction

2.1 Photometric observations

The first almost complete multi-colour light curves of V404Aur in Johnson minus;Cousin BVR_cI_c filters (Ažusienis & Straižys 1969; Bessell 1983) were observed on January 1, 2, and 3, 2023, with the Andor DZ936 2K CCD (size: 2 048 × 2 048 pixel) photometric system attached to the 85 *cm* telescope at the Xinglong Station of the National Astronomical Observatories of China (NAOC). New complete Johnson minus;Cousin VR_cI_c (Ažusienis & Straižys 1969; Bessell 1983) multi-colour light curves of GW Gem were observed on December 25 and 26, 2022. The a observations were accomplished with the PI VersArray 1300B LN CCD (size: 1 340 × 1 300 pixels) photometric system attached to the 80 cm telescope (Tsinghua-NAOC Telescope) at NAOC. PHOT package of IRAF was used to process all the observation images. The comparison stars and the check stars have been chosen to determine the differential magnitudes. The non-variable star TYC 2924-2022-1 and TYC 2924-1540-1 are chosen as comparison star and the check star for V404 Aur, respectively. Meanwhile, the star TYC 1933-570-1 and 2MASS J07521442+2705257 are chosen as comparison stars, and the star 2MASS J07521241+2703288 is chosen as the check star for GW Gem. Table 1 shows the information of comparison, check stars and both targets. The comparison stars have similar magnitudes to the targets. The observed CCD images of both targets are shown in Figs. 1 and 2, respectively. In the figure, the variable star is marked with 'V', the comparison star is marked as 'C', and the check star is marked with 'Ch,' respectively. Especially, the two comparison stars for GW Gem were marked as 'C1' and 'C2' in Fig. 2. The light curves of V404 Aur and GW Gem are shown in Figs. 3 and 4, respectively. The magnitude difference between the comparison star and the check star in all filters is shown at the bottom of the figure. In Fig. 3, the mean standard deviations of each filter are about 0.00452 of the B band, 0.00454 of the V band, 0.00559 of the R_c band and 0.00994 of the I_c band. In Fig. 4, the mean standard deviations of each filter are about 0.00454 of the V band, 0.00559 of the R_c band, and 0.00994 of the I_c band.

2.2 TESS observations

The Transiting Exoplanet Survey Satellite (TESS) is an all-sky transit survey whose principal goal is to detect Earth-sized planets orbiting bright stars amenable to follow-up observations to determine planet masses and atmospheric compositions (Ricker et al. 2014). TESS conducted high-precision photometry of more than 200 000 stars during its primary two-year mission with a cadence of approximately 2 min and 20 s in the extended mission for select targets. These targets are recorded as postage stamps and made available to the community as target pixel files (TPFs) and calibrated light curves. The light curve files contain the flux time series derived from the calibrated 2-min and 20-s target pixels. These files contain several time series, including the simple aperture photometry, a detrended light curve, position vectors, and quality flags. The aperture photometry flux series is known as the SAP_FLUX, while the flux series that has the common instrumental systematics removed using the CBV files is known as the PDCSAP_FLUX. The PDCSAP_FLUX light curves also correct for the amount of flux captured by the photometric aperture and crowding from known nearby stars.

https://doi.org/10.1017/pasa.2024.115 Published online by Cambridge University Press

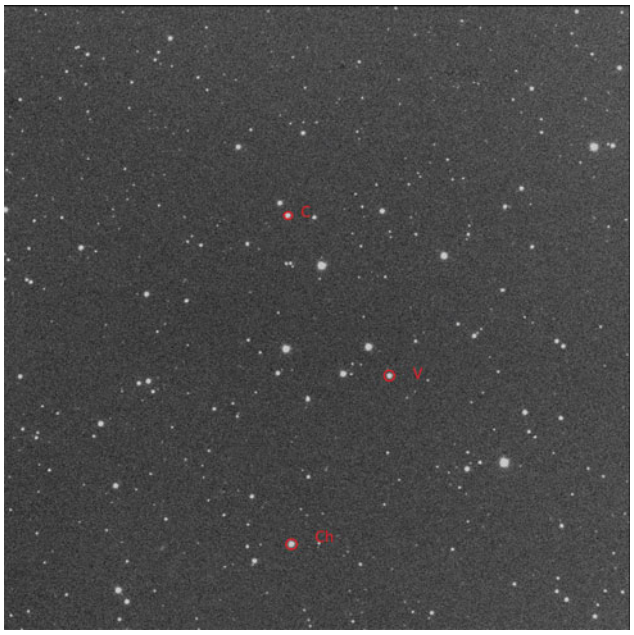

Figure 1. Observed CCD image of V404 Aur. The data observed on different night are marked with different colours, and the B, V, R_c, and I_c band data are represented by the square, circle, triangle, and inverted triangle, respectively. 'Variable star', 'Comparison star', and 'Check star' are marked with 'V', 'C' and 'Ch,' respectively.

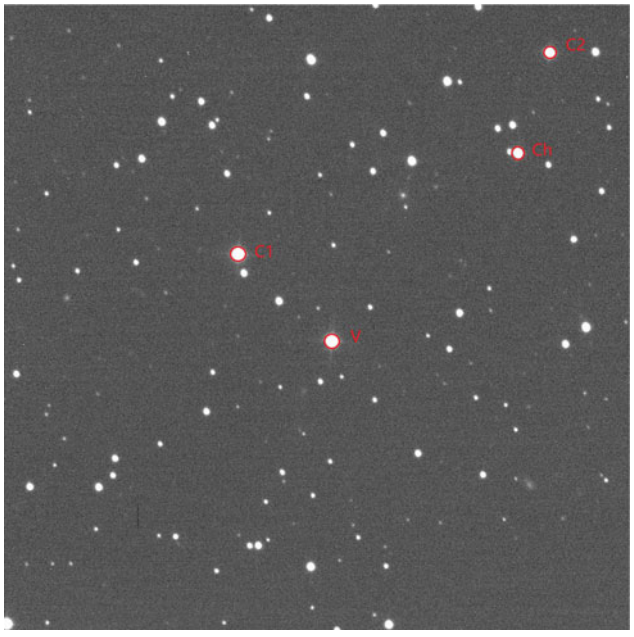

Figure 2. Observed CCD image of GW Gem. The data observed on different night are marked with different colours, and the B, V, R_c, and I_c band data are represented by the square, circle, triangle, and inverted triangle, respectively. 'Variable star', 'Comparison star', and 'Check star' are marked with 'V', 'C' and 'Ch,' respectively.

V404 Aur (TESS target identifier: TIC 440362600) and GW Gem (TIC 126218852) are members of the TESS Input Catalog (TIC) which were used to select targets to observe at the 2-min cadence. V404 Aur and GW Gem were initially monitored during the TESS Prime Mission in some sectors, the detailed information of the TESS data used in this study of both targets was listed in

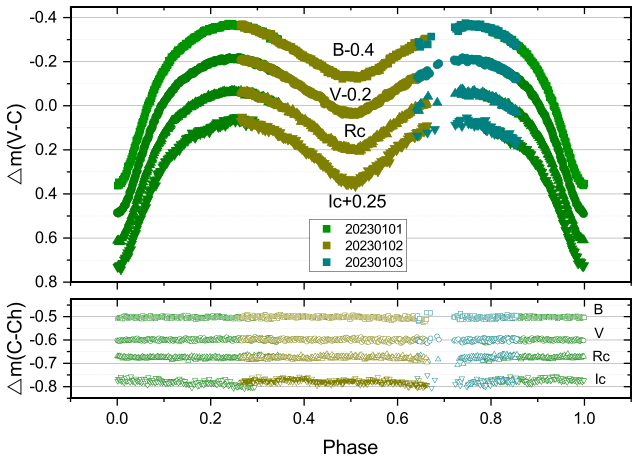

Figure 3. The light curves of V404 Aur on BVR_cI_c bands. The data observed on different night are marked with different colours, and the B, V, R_c, and I_c band data are represented by the square, circle, triangle, and inverted triangle, respectively.

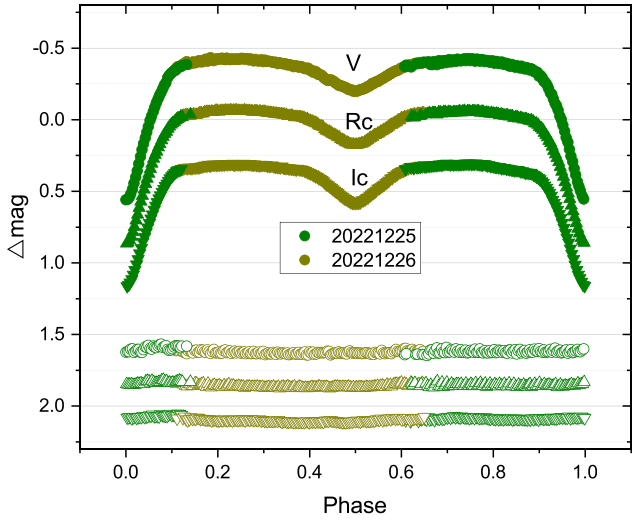

Figure 4. The light curves of GW Gem on VR_cI_c bands. The data observed on different night are marked with different colours, and the V, R_c, and I_c band data are represented by the circle, triangle, and inverted triangle, respectively.

the Table 2, which includes the sector, provenance name, exposure time, and observation time. The data were retrieved using the Python package lightkurve (Lightkurve Collaboration et al. 2018) from the MAST data archive(http://https://mast.stsci.edu/), which provides three different types of data products. Two kinds of light curves from the authors named TESS-SPOC and QLP, and the other is the TESScut cutouts of the calibrated Full Frame Images from the author named TESScut with an exposure time of 158.4 s. We downloaded 20×20 pixels files centered on V404 Aur and GW Gem using the TESScut tool. Then, the python procedure *dat.to_lightcurve* was used to get a simple aperture photometry light curve. The flux data are normalised. In this way, the light curves of V404 Aur from sector 59 and 73 and that of GW Gem from sector 71 and 72 were obtained. The time-series light curves of each sector and phase-binned light curves of V404 Aur and GW Gem obtained from the TESS database are presented in Figs. 5 and 6. It should be noted that these data were not compared

https://doi.org/10.1017/pasa.2024.115 Published online by Cambridge University Press

Table 2. Information of the TESS data of V404 Aur and GW Gem.

Target	TESS sector	Year	Provenance	Exptime(s)	Obstime
V404 Aur	19	2019	QLP	1 800	11.28–12.23
	59	2022	TESScut	158.4	11.30–12.09,12.14–12.23
	73	2023	TESScut	158.4	12.11–12.20,2023.12.27–2024.01.03
GW Gem	44	2021	TESS-SPOC	600	10.12–11.05
	45	2021	TESS-SPOC	600	11.07–12.02
	46	2021	TESS-SPOC	600	12.03–12.30
	47	2021	TESS-SPOC	600	2021.12.31–2022.01.27
	71	2023	TESScut	158.4	10.19–10.28,11.01–11.10
	72	2023	TESScut	158.4	11.15–11.24,11.27–11.30

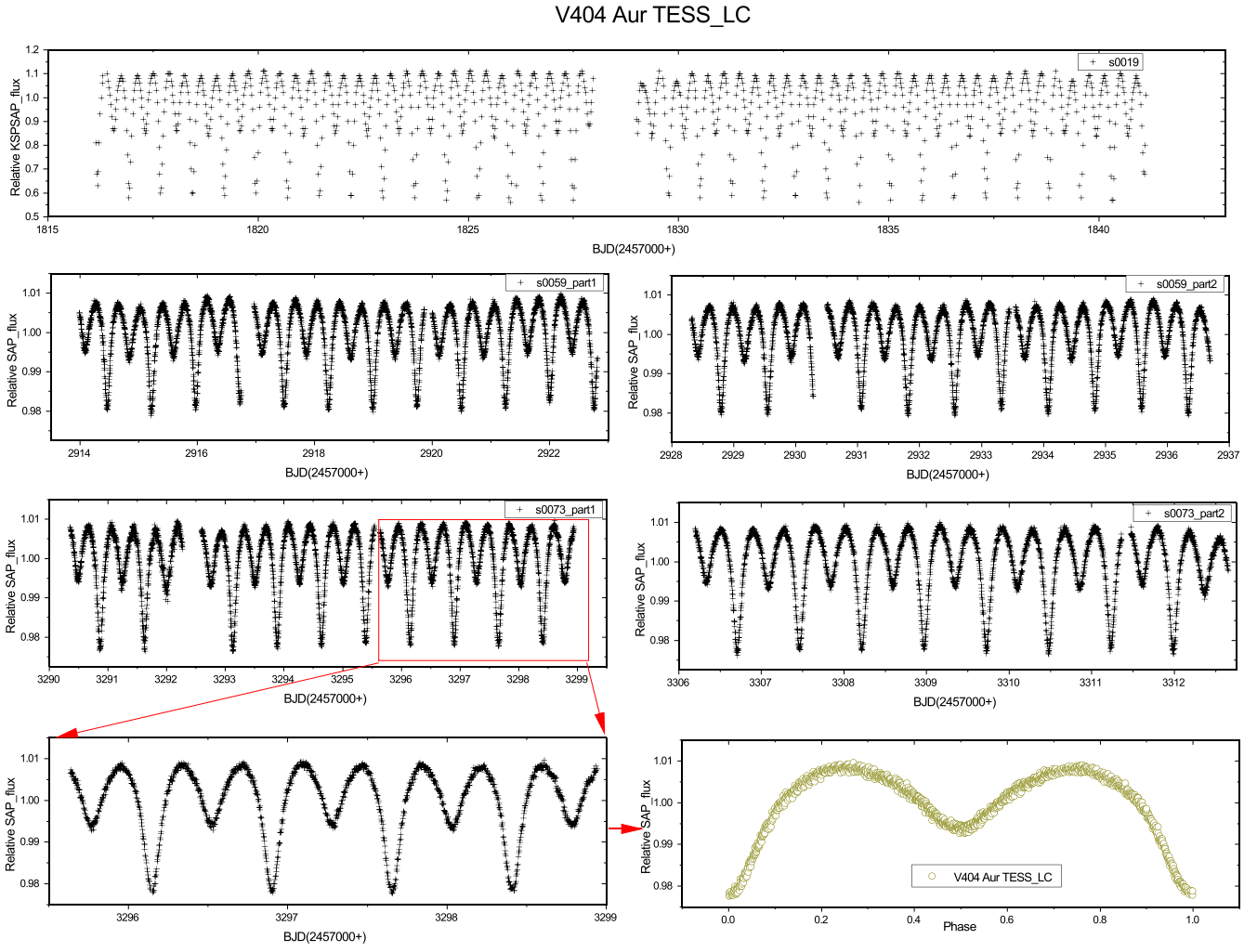

Figure 5. The continuous time-series and phase-binned light curves of V404 Aur obtained from TESS database.

to a constant star to make them differential. The phase-binned light curves of both targets were based on the part of the data in corresponding sectors, which were shown in the left panel of the phase-binned light curves individually.

2.3 Spectroscopic observations

The spectra of V404 Aur and GW Gem were observed with the Beijing Faint Object Spectrograph and Camera (BFOSC) mounted to the 2.16m telescope of Xinglong station of the National

https://doi.org/10.1017/pasa.2024.115 Published online by Cambridge University Press

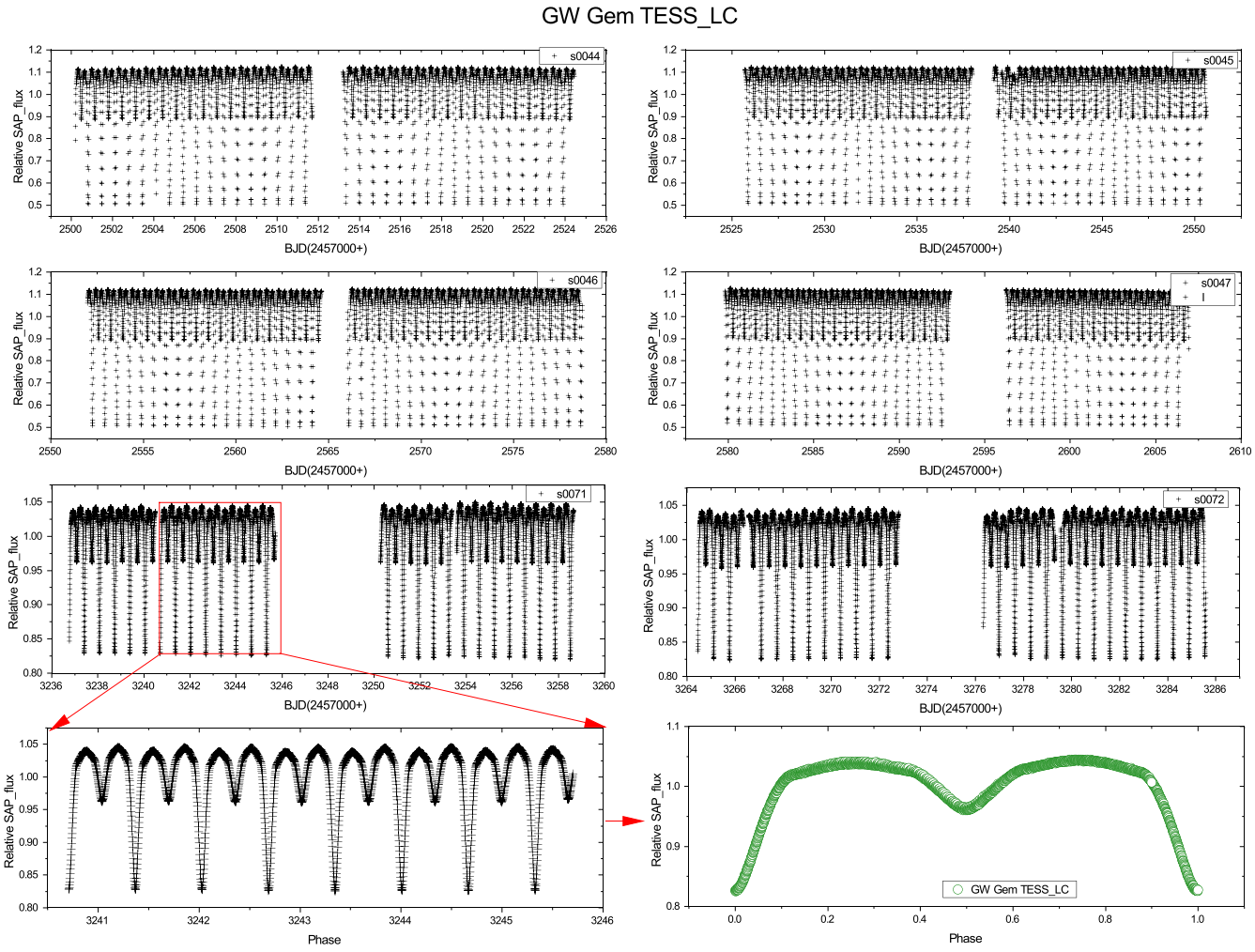

Figure 6. The continuous time-series and phase-binned light curves of GW Gem obtained from TESS database.

Astronomical Observatories of China (NAOC), Chinese Academy of Sciences (CAS). Two spectra of V404 Aur were observed on 2023 November 14 and 15, and one spectrum of GW Gem was observed on 2023 November 15. Low-dispersion spectrometer BFOSC and grism G6 were used during our observation. The slit width and line dispersion of grism G6 are 1.8 arcsec and 88 Å mm^{-1}, respectively, and the observation wavelength range is 330–545 nm (Fan et al. 2016). The spectra resolution is 1.98 Å per pixel. IRAF was used to process the observation images and extract the spectra. Normalised flux was obtained with atmospheric absorption lines corrected. In such resolution, spectra can only show the spectral lines of the primary star, and the lines of the secondary star may be too faint to be detected. The observed spectrum is shown in Fig. 7 with black lines.

University of Lyon Spectroscopic analysis Software (ULySS) (Koleva et al. 2009) was employed to acquire the atmospheric parameters through full spectra fitting with model spectra generated by an interpolator with the ELODIE library (Prugniel & Soubiran 2001). The red lines in Fig. 7 show the fitted spectra. The atmospheric stellar parameters were derived, for V404Aur: T_{eff} = 8483±273 K, log g=3.94±1.40 cm/s^2, [Fe/H]=-0.57±0.17 dex; for GW Gem: T_{eff}=7455±218 K, log g=4.11±0.60 cm/s^2, [Fe/H]=-0.26±0.10 dex. Since, for the above two targets, in the spectra analysis program, the binaries spectra were analysed as the single star spectra ignoring the secondary (faint) component, it might happen that diluted primary's spectra mimic a low metallicity. Commonly, the atmospheric parameters obtained by ULySS can be used to describe the atmospheric characteristics of the primary star. The physical properties of the primary can be estimated from the atmosphere parameters by matching with stellar isochrones (Zhang et al. 2019), using the PARSEC (PAdova and TRieste Stellar Evolution Code) isochrone database (Bressan et al. 2012; Chen et al. 2014, 2015; Tang et al. 2014), along with the lognormal form initial mass function by Chabrier (2001). Then the primary stars' physical properties (including mass, radius, and age) can be determined. For V404Aur: $M_1 = 1.72^{1.77}_{1.68}$ $M_\odot$, $R_1 = 2.29^{2.53}_{2.19}$ $R_\odot$, $logL_1 = 1.388^{1.469}_{1.341}$ $L_\odot$; for GW Gem: $M_1 = 1.47^{1.52}_{1.43}$ $M_\odot$, $R_1 = 1.76^{1.85}_{1.69}$ $R_\odot$, $logL_1 = 0.939^{1.007}_{0.869}$ $L_\odot$.

The blue-violet spectrum (3 800–4 600 Å) of V404 Aur, GW Gem and part of the spectrum of two MK standard spectra with a type of A3 V (Bet Leo) and F0 III are shown in Fig. 8. It is clear that the Ca II K lines of V404 Aur and GW Gem are quite weaker in strength than that of the A3 and F0 MK standards.

https://doi.org/10.1017/pasa.2024.115 Published online by Cambridge University Press

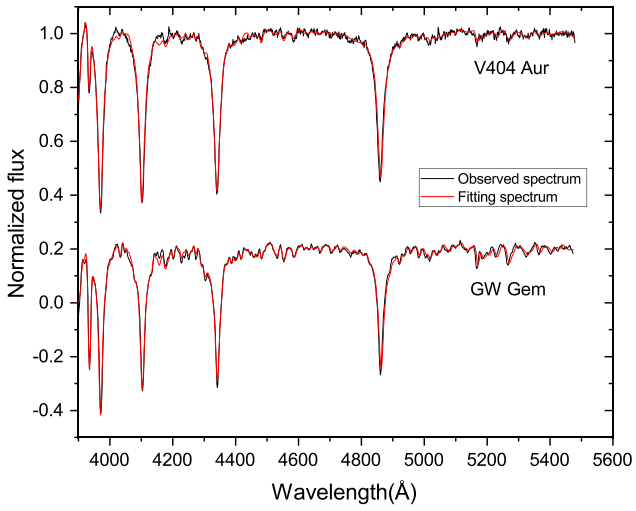

Figure 7. Spectrum of V404 Aur and GW Gem observed on 2023 November 15. The black and red lines in the top panel represent the observed and fitted spectrum, respectively.

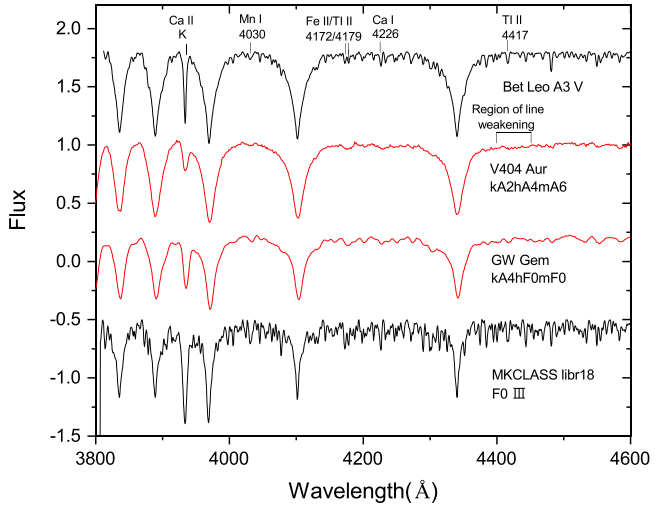

Figure 8. A comparison of the blue-violet spectrum (3 800–4 600 Å) of V404 Aur and GW Gem with the part of the spectrum of two MK standards.

3. *O-C* Diagram Analysis

All the available times of light minimum with error of V404 Aur and GW Gem were collected from the literature. Meanwhile, we computed the light minimums based on the TESS observation data for both targets and turned the BJD time into HJD time, which were listed in the Appendix of Tables A1 and B1 marked with 'This study*' in the corresponding reference column.

3.1 V404 Aur

For V404 Aur, combining with two eclipse timings observed by us and 137 eclipse timings obtained from the TESS data base, total 221 eclipse times crossing about 60 yr were used to structure the $O-C$ diagram. All eclipse times used for the period analysis are listed in the Appendix of Table A1. The reference items marked with '*' mean that the original publications are unavailable online.

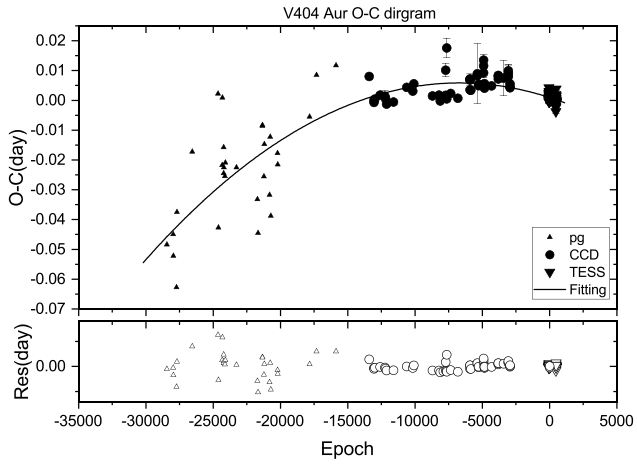

Figure 9. $O-C$ diagram of V404 Aur.

The corresponding $O-C$ and cycles E were obtained with the following ephemeris:

$$MinI = HJD\,2459946.14318 + 0.7543173^{d} \times E \quad (1)$$

The $O-C$ diagram of V404 Aur is shown in Fig. 9 with error bars, in which, triangle and circle dot represent the data observed with photograph (pg), and CCD type detectors, respectively. In particular, the anti triangle was used to mark the light minimum obtained from the TESS database. A weight of 1 for photograph data and a high weight of 10 for CCD data (including the TESS-based) were applied in the $O-C$ analysis. Based on the least-squares method, the following equation can describe the $O-C$ diagram:

$$MinI = HJD\,2459956.14413(3) + 0.754315832(11) \times E - 1.10(1) \times 10^{-10} \times E^{2} \quad (2)$$

The quadratic term in the above polymerisation means that the period is undergoing a long-term decrease at a rate of $dP/dt = -1.06(\pm 0.01) \times 10^{-7}$ d yr^{-1}. The black line in Fig. 9 represents the corresponding fitted curve. The fitting residuals are shown at the bottom of Fig. 9, and there is no cyclic change and other change anymore.

3.2 GW Gem

For GW Gem, a totally of 578 eclipse times crossing about 94 years were used to structure the $O-C$ diagram including 2 new observed and 381 eclipse timings estimated from the TESS data base by this study, which are listed in the Appendix of Table B1. The following ephemeris is used to obtain the corresponding $O-C$ and cycle E.

$$MinI = HJD\,2459939.34201 + 0.659444013^{d} \times E \quad (3)$$

Fig. 10 shows the $O-C$ diagram with the error bar of GW Gem, in which pentagram, triangle, square, and circle dot represent the data observed with visual (vis), photograph (pg), photoelectricity (pe) and CCD type detectors, respectively. The light minimum obtained from the TESS database was marked with the

https://doi.org/10.1017/pasa.2024.115 Published online by Cambridge University Press

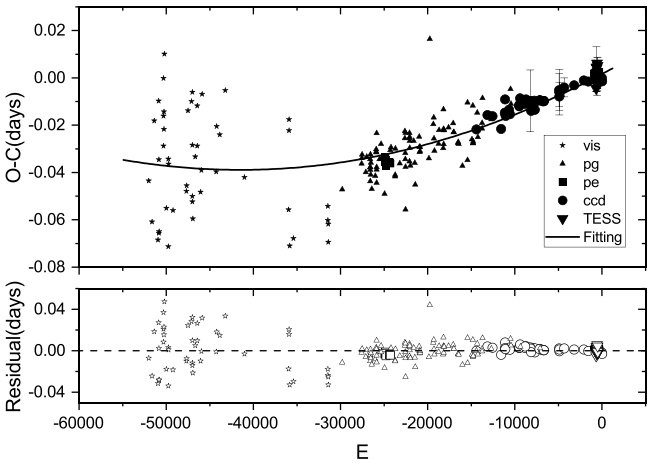

Figure 10. $O-C$ diagram of GW Gem.

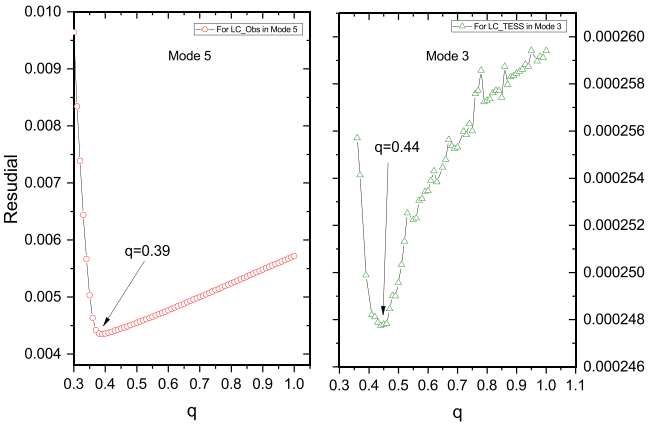

Figure 11. $\sum$-q curves of V404 Aur.

same anti-triangle as shown in Fig. 9. In the $O-C$ analysis program, the weights adopted for each observation method data are shown as follows: 1 for visual (vis) and photographic (pg) data, 10 for photoelectric (pe) and CCD data. Based on the least-squares method, the $O-C$ of GW Gem can be described by the following equation:

$$\begin{aligned} MinI = {} & HJD\,2459939.34318(2) \\ & +0.659445886(5) \times E \\ & +2.18(1) \times 10^{-11} \times E^2 \end{aligned} \quad (4)$$

The quadratic term in the above polymerisation means that the period is undergoing a long-term increase at a rate of $dP/dt = +2.41(\pm 0.01) \times 10^{-8}$ d yr^{-1}, which is consistent with the analysis of Lee et al. (2009). The black line in Fig. 10 represents the corresponding fitted curve. The fitting residuals are shown at the bottom of Fig. 10.

4. Light Curve Analyses

4.1 V404 Aur

The first multi-colour light curves of V404 Aur were observed. The TESS observation data from sector 73 (covering about HJD 2460595.5 to HJD 2460299.0) was utilised to generate the light curve for analysis, which is shown in the bottom right panel of Fig. 5. In the figures below, the observed multi-colour light curve is labeled as 'LC_Obs', while the light curve obtained from the TESS database is labeled as 'LC_TESS'. Different linear ephemerides were used to calculate the phased light curves. For the multi-colour light curves, the following linear ephemeris was employed.

$$\begin{aligned} MinI = {} & HJD\,2459946.14318(29) \\ & +0.7543173^d \times E \end{aligned} \quad (5)$$

For the light curve form TESS, following linear ephemeris was used:

$$\begin{aligned} MinI = {} & HJD\,2460296.14608(23) \\ & +0.7543173^d \times E \end{aligned} \quad (6)$$

in which, the epoch 2459946.14318(29) is the observed eclipse times and 2460296.14608(23) is the eclipse times based on the TESS database.

Wilson-Devinney (W-D) program (Wilson & Devinney 1971; Wilson 1990, 2012) was used to analysis the two sets of light curves. The effective temperature of the primary star was obtained as $T_1 = 8\,483$ K from our spectral analysis and the primary effective temperature was fixed at 8 483 K in the WD process. The gravity-darkening coefficients and bolometric albedos for the both components with radiative envelope ($T > 7\,200$ K) are taken as g_1=1, $g_2 = 0.32$ and A_1=1, $A_2 = 0.5$ (Ruciński 1969). Meanwhile, the bandpass limb-darkening coefficients taken from van Hamme (1993) and the logarithmic bolometric coefficients were applied. We acquired the convergent solutions of LC_Obs with Mode 5 (the semidetached case with the secondary component filling the critical RL). The corresponding adjustable parameters of Mode 5 are following: the monochromatic luminosity of star 1, L_{1B}, L_{1V}, L_{1R_c}, L_{1I_c}; the orbital inclination i; the mean temperature of star 2, T_2; and the dimensionless potential of the primary star, Ω_1. Based on the TESS light curve, we determined that there is no convergent solution when $q > 0.45$ with Mode 5, and there is no convergent solution when $q < 0.36$ with Mode 3. Therefore, the convergent solution with Mode 3 would be more suitable for the LC_TESS of this target. The adjustable parameters in the Mode 3 are the same as those in the Mode 5. For confirming a more reliable mass ratio, the photometric solutions based on a group of assumed mass ratio values from 0.01 to 1 were obtained with the differential correction program. The search step length is 0.01. For all assumed values of q, the sums of weighted square deviations ($\sum (O-C)_i^2$) based on two sets of light curves are displayed in Fig. 11. In order to make the minimal q value more obvious, only the trend of change from $q = 0.3$ to $q = 1$ was plotted. The minimal value achieved at $q = 0.38$ and $q = 0.44$ for observed multi-colour light curves and TESS light curves, respectively. So we make q as an adjustable parameter and set $q = 0.38$ and $q = 0.44$ as the initial value in the WD process for the two sets of light curves, respectively. The theoretical light curves for multi-colour light curves and TESS light curve are shown in Figs. 12 and 13 in black lines, respectively. The theoretical light curves fitted the light curves very well. All converged photometric solutions are listed in Table 2. V404 Aur is likely a marginal contact binary with a extremely small contact degree of $f = 3.16\%$. It's worth noting

https://doi.org/10.1017/pasa.2024.115 Published online by Cambridge University Press

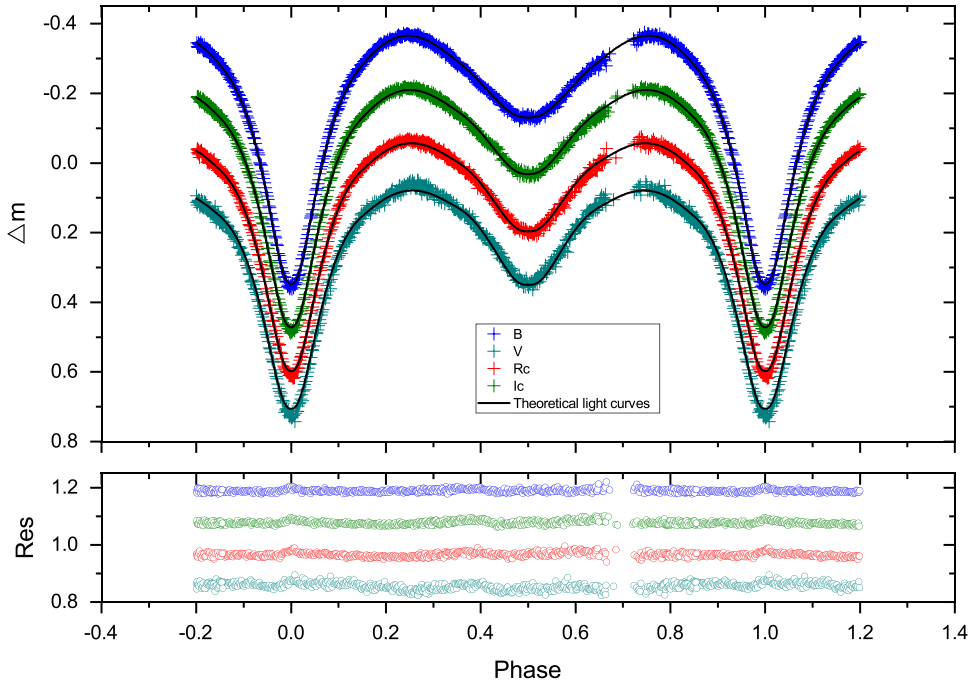

Figure 12. The theoretical light curves of V404 Aur based on multi-colour light curves with Mode 5.

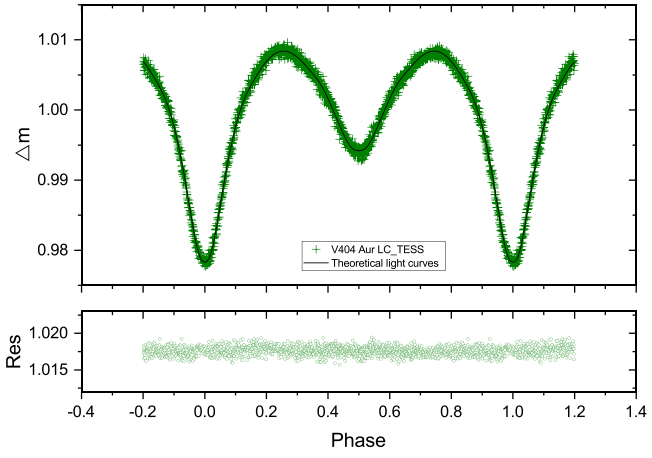

Figure 13. The theoretical light curves of V404 Aur based on TESS database with in Mode 3.

that the mass and radius ratios calculated based on the LC_TESS is larger than those based on the observed light curve LC_Obs, which may be due to the limitations in the models. The 3D geometric structure based on LC_Obs with Mode5 are shown in Fig. 14.

4.2 GW Gem

The new multi-colour light curves of GW Gem were observed. The TESS observation data from sector 71 (covering about HJD 2460240.5 to HJD 2460245.8) was utilised to generate the light curve for analysis, which is shown in the bottom right panel of Fig. 6. Same as V404 Aur, different linear ephemeris were used to calculate the phased light curves for the observed multi-colour light curves and TESS observation. For multi-colour light curves, the following linear ephemeris was used:

$$MinI = HJD\,2459939.34201(36) + 0.659444013^{d} \times E \quad (7)$$

For the light curve from TESS, the following linear ephemeris was used:

$$MinI = HJD\,2460241.36901(5) + 0.659444013^{d} \times E \quad (8)$$

in the above linear ephemeris, the epoch 2459939.34201(36) is the observed eclipse times and 2460241.36901(5) is the eclipse times based on TESS database.

Meanwhile, the Wilson-Devinney (W-D) program with appropriate parameter settings (such as gravity-darkening coefficients, bolometric albedos, bandpass limb-darkening coefficients, limb-darkening coefficients, logarithmic bolometric coefficients) was used to analyse the light curves. The primary effective temperature was fixed at 7 455 K in the WD process, which was obtained from our spectra analysis. The convergent solutions were confirmed with Mode 5. The corresponding adjustable parameters have been introduced in the previous paragraph. The search for a more reliable mass ratio has also been confirmed using the same method for V404 Aur based on the two sets of light curves. The sums of weighted square deviations ($\sum (O-C)_i^2$) for all assumed values of q are displayed in Fig. 15 based on both two sets of light curves. In order to make the minimal q value more obvious, only the trend of change from $q = 0.3$ to $q = 1$ was plotted. The minimal value is attained at $q = 0.37$ for observed multi-colour light curves (labeled as 'LC_Obs' and at $q = 0.36$ for the TESS light curves (labeled as

https://doi.org/10.1017/pasa.2024.115 Published online by Cambridge University Press

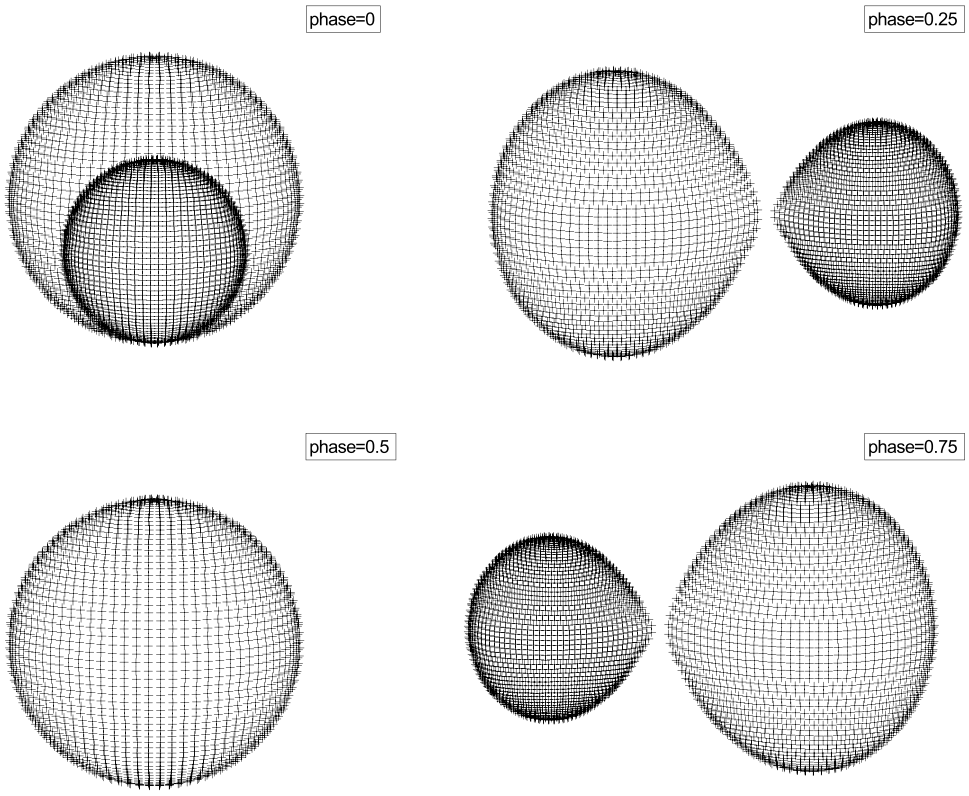

Figure 14. Geometrical structure of V404 Aur with Mode 5.

'LC_TESS'). Then 'q' was taken as an adjustable parameter and set $q = 0.37$ and $q = 0.36$ as the initial value in the WD process for the two sets of light curves, respectively. The theoretical light curves for multi-colour light curves are shown in Fig. 16 in black lines. For the light curve of TESS data, the initial theoretical light curve shows a poor fit for the two light maximum. The TESS light curve shows slight asymmetry, which can due to the brightness enhancement at the secondary light maximum or the brightness weaken at the primary light maximum. The asymmetry means that the light curves have been disturbed by some perturbation caused by the photosphere activity of the components. The discrepancies can be modeled by a possible hot spot on the primary star due to impact from mass transfer between the components, or a cool spot on the secondary star having a convective atmosphere. Thus, two different model spots were postulated to reanalyse the TESS light curves by using the unspotted photometric parameters as initial values. A spot model was employed for the light curve fit with four adjustable parameters: the latitude of spot center (θ) in degree; the longitude of spot center (ϕ) in degrees; the spot angular radius (r) in radians; and the spot temperature fact T_f ($T_f = T_s/T_*$, in which T_s is the spot temperature and T_* is the photosphere surface temperature of the star). Two kinds of spotted model have obtain the convergent solutions. While, the theoretical light curve with a cold spot didn't improve the initial fill of the secondary light maximum well. Then, the spot mode with a hot spot was considered to be more suitable. The initial theoretical light curve without spot and the theoretical light curves with a hot spot were plotted in Fig. 17 as the blue and red lines, respectively. The spotted theoretical light curves with a hot spot fitted the light curve better than the initial theoretical light curve without a spot. All converged photometric

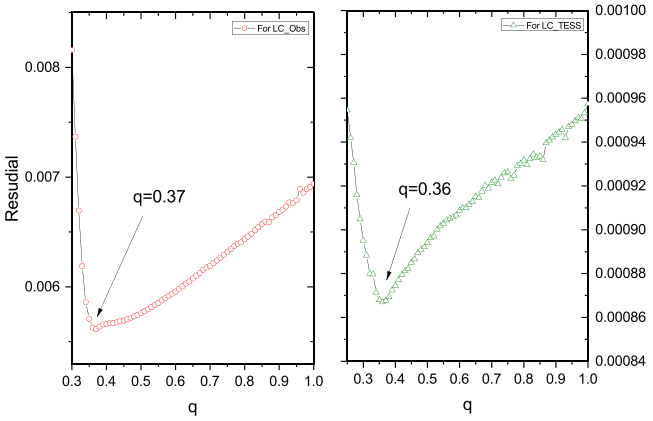

Figure 15. $\sum$-q curves of GW Gem.

solutions are listed in Table 3. The geometric structure based on LC_Obs and LC_TESS with a hot spot in 3D view are both shown in Fig. 18.

5. Discussion and conclusion

5.1 V404 Aur and GW Gem

Through the spectra analysis, the atmosphere parameters of the primary components of the two targets are obtained, which

https://doi.org/10.1017/pasa.2024.115 Published online by Cambridge University Press

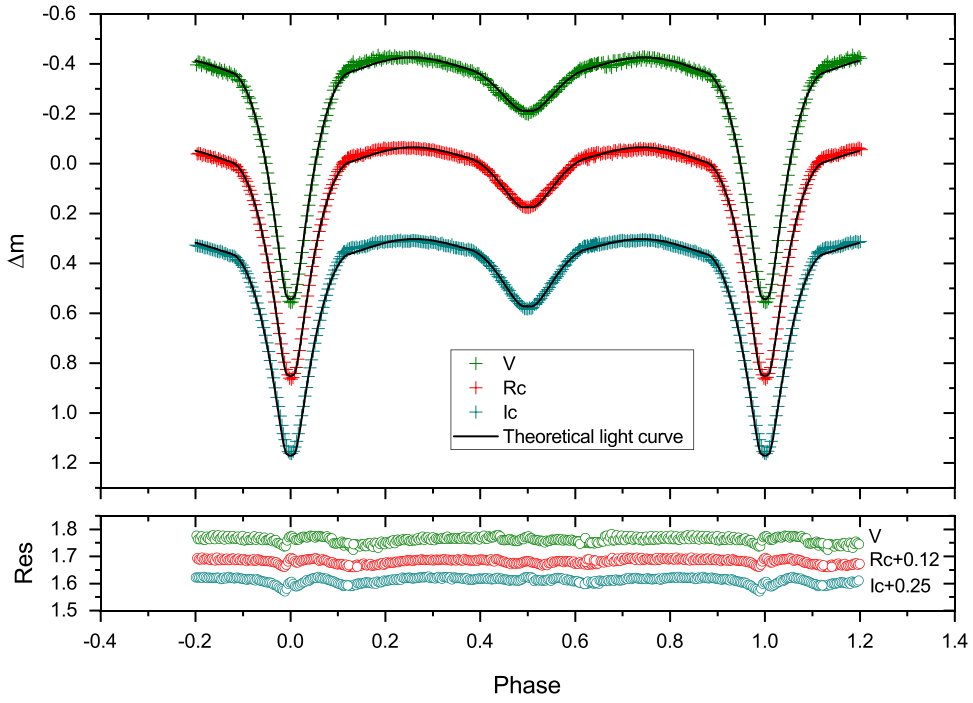

Figure 16. The theoretical light curves of GW Gem based on multi-colour light curves.

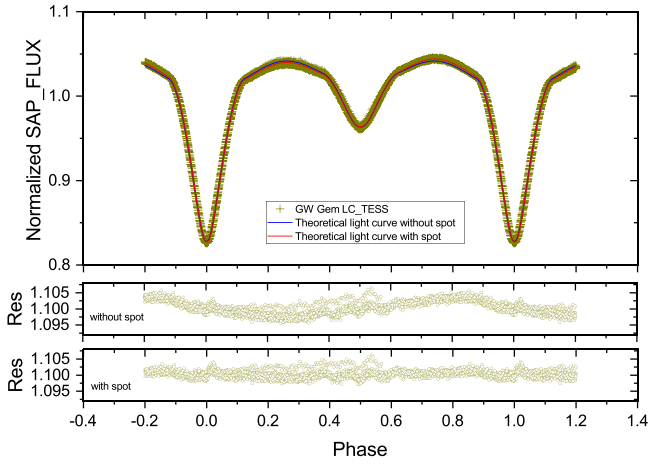

Figure 17. The theoretical light curves of GW Gem based on TESS database.

are shown as follows: for V404Aur: $T_{eff} = 8\,483\pm273$ K, $\log g = 3.94\pm1.40$ cm/s^2, [Fe/H]=-0.57±0.17 dex; for GW Gem: $T_{eff} = 7\,455\pm218$ K, $\log g$=4.11±0.60 cm/s^2, [Fe/H]=-0.26±0.10 dex. The physical properties of the primary can be estimated from the atmosphere parameters by matching with stellar isochrones, using the PARSEC database. For V404Aur: $M_1 = 1.72^{1.77}_{1.68}$ M$_\odot$, $R_1 = 2.29^{2.53}_{2.19}$ R$_\odot$, $logL_1 = 1.388^{1.469}_{1.341}$ L$_\odot$; for GW Gem: $M_1 = 1.47^{1.52}_{1.43}$ M$_\odot$, $R_1 = 1.76^{1.85}_{1.69}$ R$_\odot$, $logL_1 = 0.939^{1.007}_{0.869}$ L$_\odot$. WD program was used to fit the light curves of the two targets. The light curves of V404 Aur show *beta* Lyrae characteristics, while the light curves of GW Gem show Algol characteristics. The theoretical light curves with Mode 5 and Mode 3 fitted the LC_Obs and LC_TESS of V404 Aur quite well. The fill-degree factor of the primary component of V404 Aur is 0.9966(10) based on LC_Obs with Mode 5 and the contact degree of $f = 3.16\%$ with Mode 3, which indicates that V404 Aur should be a marginal contact binary with secondary has already filled its RL and the primary is nearly filling the RL. While the fill-degree factor of the primary component of GW Gem is 0.8098(18) based on multi-colour light curves solutions, indicating that GW Gem is a semi-detached binary with the secondary has already filling its RL. The orbital inclinations of two targets are $i = 81.11(12)°$ for V404 Aur and $i = 86.07(21)°$ for GW Gem, which means that the photometric solutions can be reliable. Based on the physical properties of the primary and the photometric solutions, the absolute parameters of the two binaries were estimated and listed in Table 4.

The light curve of TESS data shows a slight asymmetry with brightness difference between the two light maximums. Such asymmetry refers to the O'Connell effect, which is a phenomenon where the magnitude of the primary light maximum (near 0.25 phase) differs from the secondary one (near 0.75 phase) (e.g., Milone 1969; Liu & Yang 1999; Qian et al. 2014), The O'Connell effect can be caused by many common and complex mechanisms in eclipsing binaries, including flares, spots, mass transfer, etc. The spotted theoretical light curve fitted the LC_TESS of GW Gem better than the theoretical light curve without a spot. The final converged photometric solutions show that the brightness enhancement can be explained by the appearance of a hot spot near the facing surface of the primary component due to the mass transfer. Accretion stream caused by the long-term mass transfer from the secondary star will emerge on the surface of the primary component and then it will move to one side of the midline of the two stars, which will lead to local brightness enhancement of the surface (Hilditch et al. 1997). The latitude and longitude of the spot center are about 163.1° and 78.9°, and the angular radius of the spot is about 20.05°. The proportion of

https://doi.org/10.1017/pasa.2024.115 Published online by Cambridge University Press

Table 3. Photometric solutions of V404 Aur and GW Gem.

	V404 Aur		GW Gem	
	LC_Obs	LC_TESS	LC_Obs	LC_TESS hot spot
Parameters	Values	Values	Values	Values
Mode	5	3	5	5
g_1	1.0	1.0	1.0	1.0
g_2	0.32	0.32	0.32	0.32
A_1	1.0	1.0	1.0	1.0
A_2	0.5	0.5	0.5	0.5
q (M_2/M_1)	0.3749(16)	0.4400(10)	0.3666(26)	0.3531(10)
$T_1(K)$	8 483	8 483	7 455	7 455
$T_2(K)$	5496(9)	5343(14)	5105(11)	4930(3)
$i(^\circ)$	81.11(12)	83.46(27)	86.07(21)	84.530(66)
Ω_1	2.6546(33)	2.75022(29)	3.0763(54)	3.0509(23)
Ω_2	2.6264	2.75022	2.6093	2.58077
fillout factor	–	0.0316(11)	–	–
L_1/L_{totalB}	0.96500(2)	–	–	–
L_1/L_{totalV}	0.93767(4)	–	0.90288(13)	–
L_1/L_{totalR_c}	0.91489(6)	–	0.87457(19)	–
L_1/L_{totalI_c}	0.88928(10)	–	0.84642(27)	–
$L_1/L_{totaltess}$	–	0.896540(90)	–	0.872508(50)
$r_1(pole)$	0.43274(36)	0.42633(16)	0.36610(67)	0.36771(23)
$r_1(side)$	0.46121(44)	0.45431(23)	0.37957(78)	0.38129(27)
$r_1(back)$	0.48594(45)	0.48215(37)	0.38982(88)	0.39133(29)
$r_2(pole)$	0.27776(32)	0.29121(40)	0.27591(54)	0.27315(21)
$r_2(side)$	0.28947(34)	0.30393(50)	0.28751(57)	0.28459(22)
$r_2(back)$	0.32217(34)	0.33749(89)	0.32022(57)	0.31731(22)
latitude(*deg*)	–	–	–	163.1(9)
longitude(*deg*)	–	–	–	78.9(9)
radius(*radian*)	–	–	–	0.35(1)
$T_f(T_s/T_0)$	–	–	–	1.24(2)
R_2/R_1	0.64552(53)	0.68591(81)	0.7810(12)	0.76979(43)
$f(fill-degree)_1$	0.9966(10)	–	0.8098(18)	0.5268(10)
$\overline{\sum (O-C)^2}$	0.0041	0.0002	0.0052	0.0005

hot spot area in the surface of the primary component is about 2.79%. That is much larger than that of a spot on the Sun (the area of sunspot is usually less than 1% of the photospheric surface of the Sun). The spot may be composed of a group of small spots. The hot spot is one kind of vestige of mass transfer, and its area can be considered as an indirect measurable parameter of mass transfer. Moreover, the long-term orbital period increase, lasting about 100 yr, is further evidence of mass transfer between components.

It is noteworthy that the light curves observed by Broglia & Conconi (1981) from 1978 to 1979 show no obvious asymmetry. However, Lee et al. (2009) detected asymmetric in the muticolour light curves observed around 2007 2008. The difference in brightness between the sets of light curves has not yet understood. A trifling hot spot may be present because of the weak mass transfer. This spot might be relatively inconspicuous, and its impact on the light curves is smaller than the measurement precision.

All available eclipse times were used to investigate the variations of the orbital period by analyzing the $O-C$ diagram. The $O-C$ analysis found that the period of V404 Aur is decreasing at a rate of $dP/dt = -1.06(\pm 0.01) \times 10^{-7}\,\mathrm{d\,yr^{-1}}$, while the period of GW Gem is increasing at a rate of $dP/dt = +2.41(\pm 0.01) \times 10^{-8}\,\mathrm{d\,yr^{-1}}$. The long-term period change was in agreement with the semi-detached configuration of the close binary system. For V404 Aur, the period decrease may mainly be caused by the combined effects of the angular momentum loss (AML) via an enhanced stellar wind of the more evolved secondary star and mass transfer between two components (e.g.,Tout & Eggleton 1988; Liao et al. 2017; Liao, Qian, & Sarotsakulchai 2019).

https://doi.org/10.1017/pasa.2024.115 Published online by Cambridge University Press

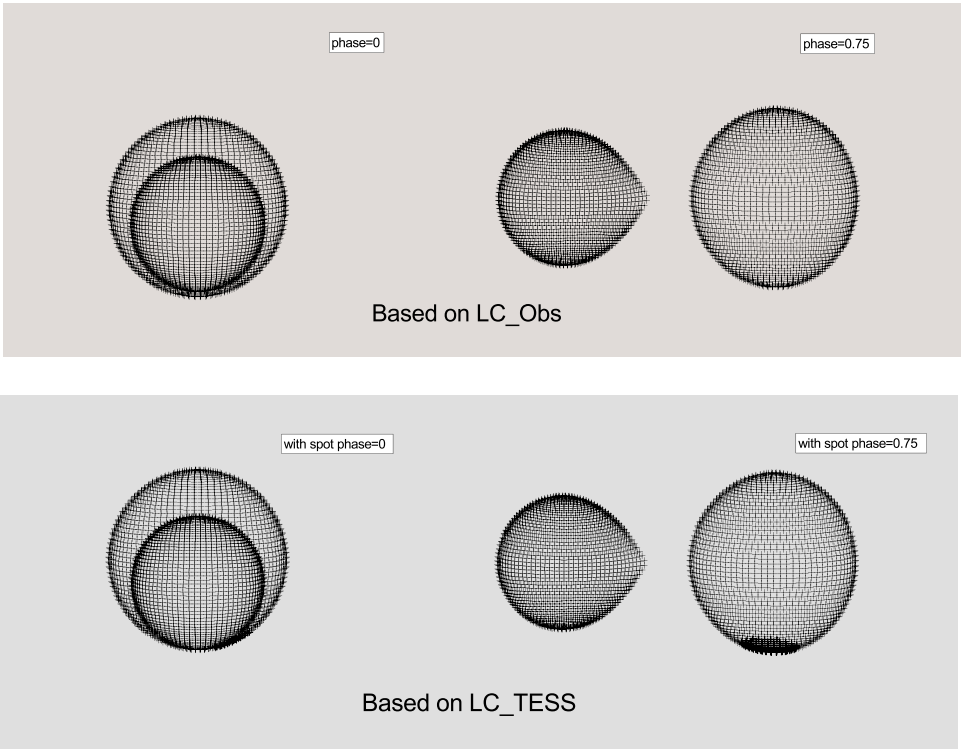

Figure 18. Geometrical structure of GW Gem.

Table 4. Absolute parameters of V404 Aur and GW Gem.

	V404 Aur	GW Gem
Parameters (Unints)	Values	Values
M_1 ($M_\odot$)	$1.72^{1.77}_{1.68}$	$1.47^{1.52}_{1.43}$
M_2 ($M_\odot$)	$0.64^{0.66}_{0.63}$	$0.54^{0.56}_{0.52}$
R_1 ($R_\odot$)	$2.29^{2.53}_{2.19}$	$1.76^{1.85}_{1.69}$
R_2 ($R_\odot$)	$1.48^{1.63}_{1.41}$	$1.37^{1.44}_{1.32}$
L_1 ($L_\odot$)	$24.43^{29.44}_{21.93}$	$8.69^{10.16}_{7.40}$
L_2 ($L_\odot$)	$1.93^{2.33}_{1.73}$	$1.25^{1.46}_{1.06}$

V404 Aur should be a particular target lying in the thermal relaxation oscillation theory (TRO) stage, like TYC 6408-989-1(Tian 2021) and other marginal contact binaries(Qian & Zhu 2002; Zhu et al. 2009, 2012). They are in a semidetached phase with the secondary star filling the RL, and V404 Aur has evolved into a marginal-contact phase with poor thermal contact (e.g.,Liao, Qian, & Liu 2012; Qian et al. 2013, 2014; Liao & Sarotsakulchai 2019), while GW Gem will evolve into such a phase. GW Gem is a typical Algol system in a semidetached phase with the secondary star filling the RL. The long-term period increase of GW Gem is in agreement with the semi-detached configuration of this system. The period increase may be the result of the mass transfer from the secondary component to the primary one (e.g., Qian 2002; Tian & Zhu 2019), resulting in a hot spot on the primary's surface. Mass transfer in the two targets additionally suggests that mass transfer may be important in the formation of Am stars.

The components in very short-period near-contact systems, such like V404 Aur and GW Gem, are likely to be rotating synchronously. For a circular orbit, the following equation can be used to obtain the equatorial rotational velocity: $v = 50.6(R/R_\odot)/(P/d)$ km s^{-1}(Carquillat & Prieur 2007), in which R is the radius of the considered component, P is the orbital period, v is its equatorial rotational velocity. The projected rotation velocity $v \sin i$ of the primaries of V404 Aur and GW Gem can be estimated as approximately 152 and 135 km s^{-1}, respectively. The targets are very special Am type eclipsing binary with very short period (less than one day) and quit large rotational velocity, which make them became a challenge to the cut-off of rotation velocities and periods of Am stars, like V1073 Cyg ($v \sin i = 150$ km s^{-1}) (Budaj 1996), and V2787 Ori ($v \sin i = 152$ km s^{-1} based on R_1=2.45 $R_\odot$ Tian, Zhu, & Wang 2019).

5.2 Properties of eclipsing Am binaries and statistical analysis

The physical parameters were collected for the well-known eclipsing Am binaries. A parameter table has been compiled and is displayed in the Appendix of Table 8. Currently, there are only 54 systems were well studied. The relationships between the parameters were also discussed. The distribution and relations between the mass ratio ($q = M_2/M_1$), radius ratio ($k = M_2/M_1$), surface effective temperature ratio (t=T_2/T_1), the luminosity ratio ($l = L_1/L_2$), and the total mass (M_{total}) were discussed and the figures were shown in Fig. 19. Different colours were used to mark the EA and EB and EW type eclipsing Am binaries. The relation between l versus q is shown in the upper left-hand panel, with

https://doi.org/10.1017/pasa.2024.115 Published online by Cambridge University Press

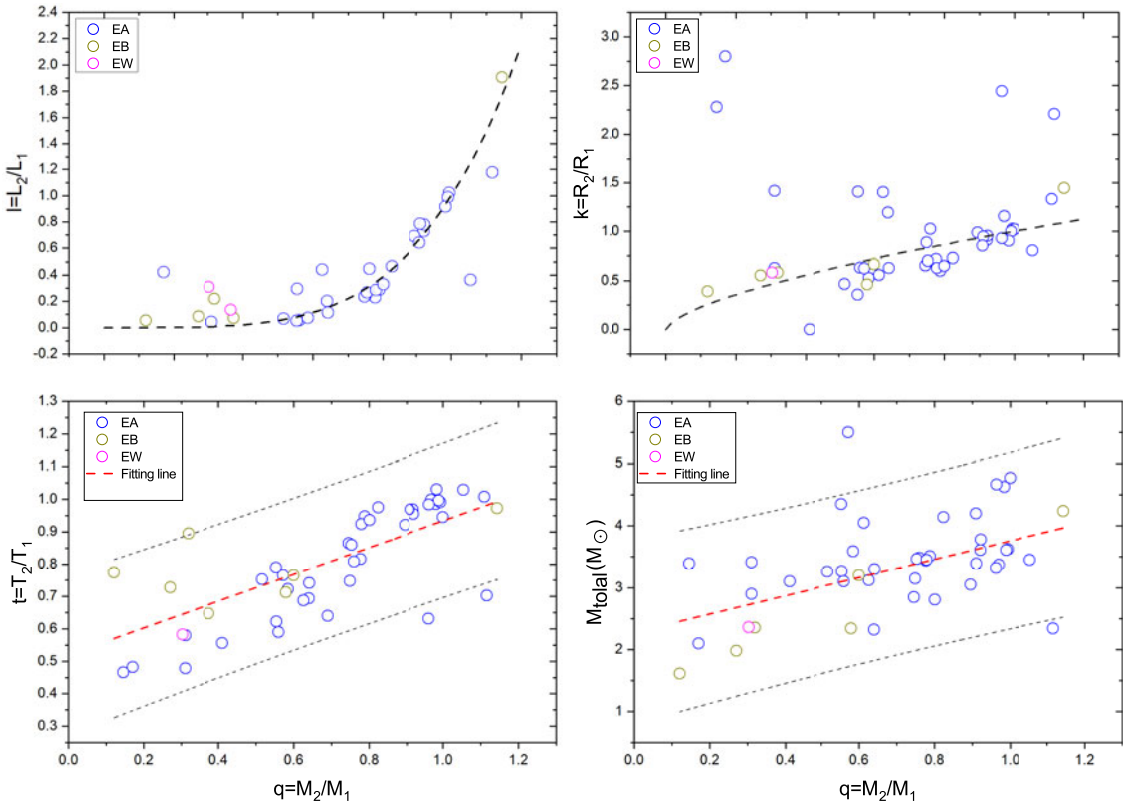

Figure 19. The relations between the mass ratio (q), radius ratio (k), effective temperature ratio (t), luminosity ratio (l), and total mass (M_{total}) of the eclipsing Am binaries. Upper left-hand panel: the l versus q; Upper right-hand panel: the k versus q. Bottom left-hand panel: the t versus q, the red dashed line is the fitting line for the EA type systems, the black dash lines represent the edges of the strip defined by the 5% and 95% percentiles of t for each q bin; Bottom right-hand panel: the M_{total} versus q, the red dashed line is the fitting line and the black dash lines are as same as that in the diagram of t versus q.

the black dashed line representing main-sequence star mass-luminosity relation(i.e. M-L relation), $l = q^{4.216}$. Most systems adhere to the main-sequence M-L relation. The diagram in the upper right-hand panel displays k versus q, with the dashed line representing the empirical mass-radius of the main-sequence star, i.e. M-R relation, $k = q^{0.64}$. The M-R distribution of eclipsing Am binaries is around the main-sequence relation. The bottom left-hand panel shows the relation between the t and q, in which one can see that the temperature ratio(t) and the mass ratio(q) of the EA type eclipsing Am binaries follows a good linear relation. Meanwhile, the total mass, M_{total} is also shown as a liner function of the mass ratio q, which is shown in the bottom right-hand panel. The two linear fitting lines can be written as follows:

$$t = 0.413(\pm 0.060) \times q + 0.520(\pm 0.045) \quad (9)$$

$$M_{total} = 1.476(\pm 0.372) \times q + 2.278(\pm 0.297) \quad (10)$$

The red dash-line in the bottom panels are the fitting lines, the black dash lines around the fitting line represent the edges of the strip defined by the 5% and 95% percentiles of t and M_{total} for each q bin. Moreover, both of the boundaries are better defined. There is no other discussion about the relation between the total mass and mass ratio of the eclipsing Am binaries. However, but some authors have published their results on the relation of the normal late-type contact binaries (i.e. W UMa systems). The relationship between the total mass and mass ratio of the W UMa systems was identified by van't Veer (1996), and has subsequently been confirmed by Li et al. (2008) based on 130 well known W UMa systems. This is further verified by Sun et al. (2020) based on 2 335 W UMa systems(1 530 W-, 710 A-, and 95 B-type CBs) obtained from the Catalina Sky Survey (CSS). The slope of the best linear fit to our sample is $dM_{total}/dq = 1.4762 \pm 0.3723$, which is larger than that of Sun et al. (2020) with a slope of 0.57 ± 0.02.

The relations between effective temperature T, mass M, radius R, and luminosity can help us to investigate the evolutionary stage of the systems. Fig. 20 shows the distributions of Hertzsprung-Russell (HR) diagram, the different symbols are used to help distinguish EA, EB, and EW type systems, while the orange and green colours mark the primary and the secondary component, respectively. One can see from Fig. 20 that the components of the systems are mainly around the zero-age main sequens, and some secondary components have evolved away from the main sequence. This is consistent with our statistics results in the previous work (Tian et al. 2023). The components of GW Gem and V404 Aur are also plotted in the HR diagram. The mass-luminosity relation, mass-radius relation, and mass-temperature relation of the components are shown in Fig. 21. Different colour were used to distinguish the primary and the secondary components, and different symbols were used to represent EA, EB, and EW type systems. The blue dash-lines are the corresponding empirical relationships of main sequence stars (Eker et al. 2018). Almost all components follow the empirical

https://doi.org/10.1017/pasa.2024.115 Published online by Cambridge University Press

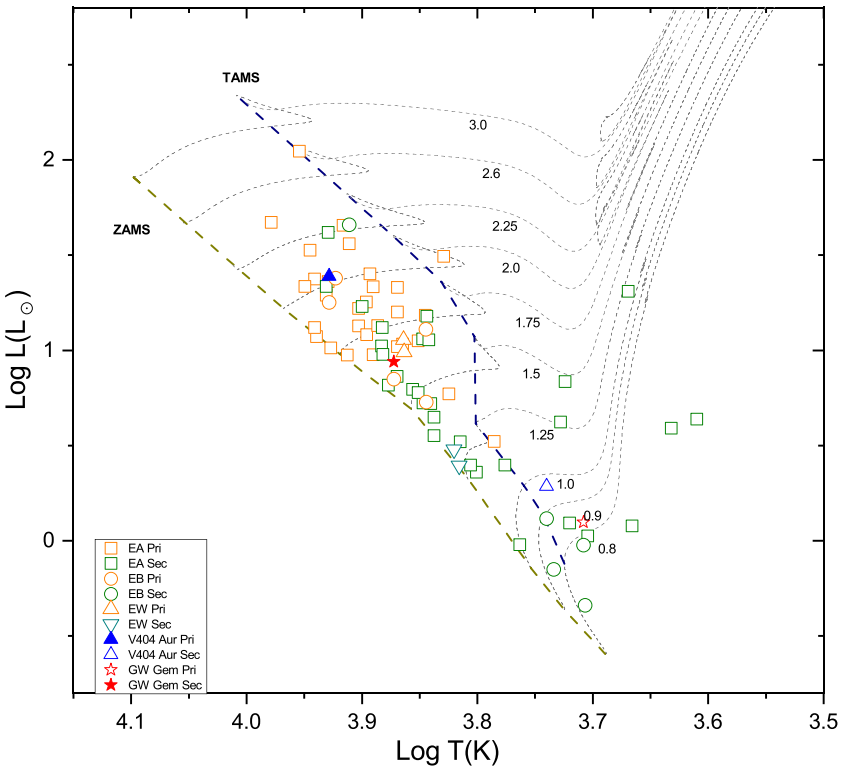

Figure 20. Hertzsprung-Russell diagram of eclipsing Am binaries. The evolutionary tracks (thin solid lines) for the labeled masses, as well as the zero-age main sequence (ZAMS) and the terminal-age main sequence (TAMS), were taken from Bressan et al. (2012), which were calculated for $Y = 0.279$, $Z = 0.017$.

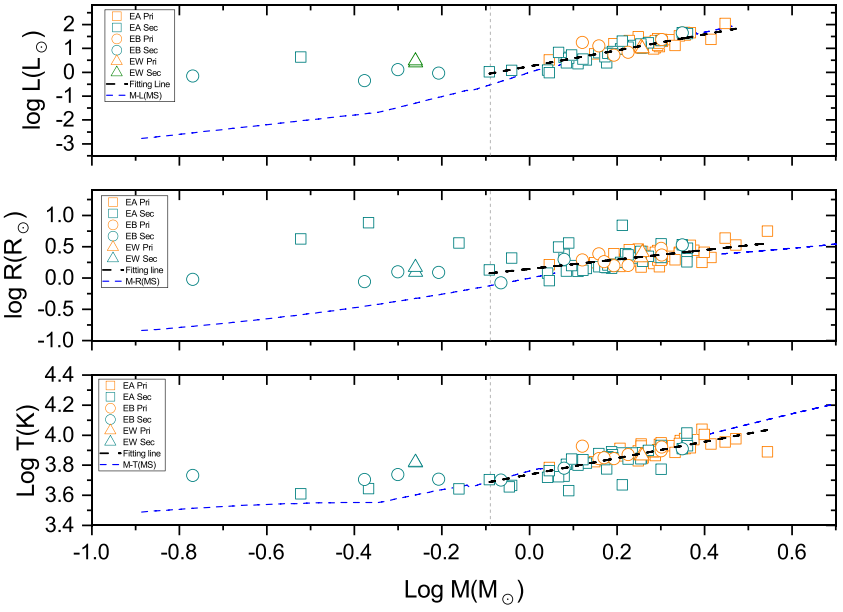

Figure 21. M-R, M-L, and M-T distribution of eclipsing Am binaries. The black dash lines in each panel are the empirical relationships of eclipsing Am binaries when $\log M > -0.09$ $M_{\odot}$. The blue dash-lines are the corresponding empirical relationships of main sequence stars (Eker et al. 2018).

https://doi.org/10.1017/pasa.2024.115 Published online by Cambridge University Press

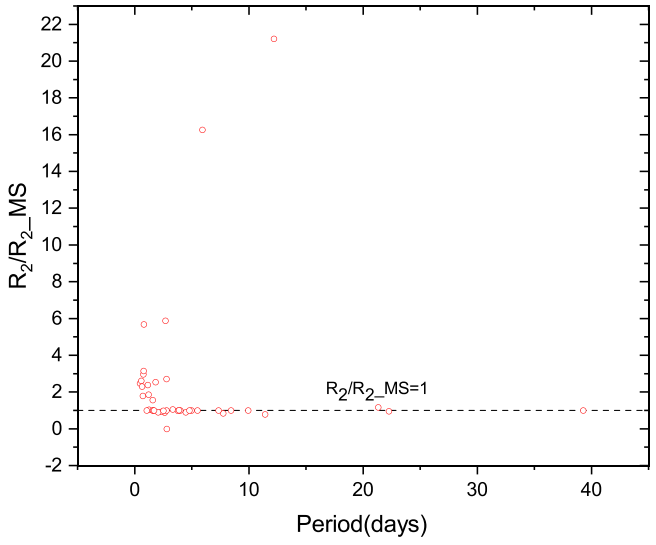

Figure 22. (R_2/R_2_MS)-Period distribution of eclipsing Am binaries. The black dash line represents R_2/R_2_MS=1.

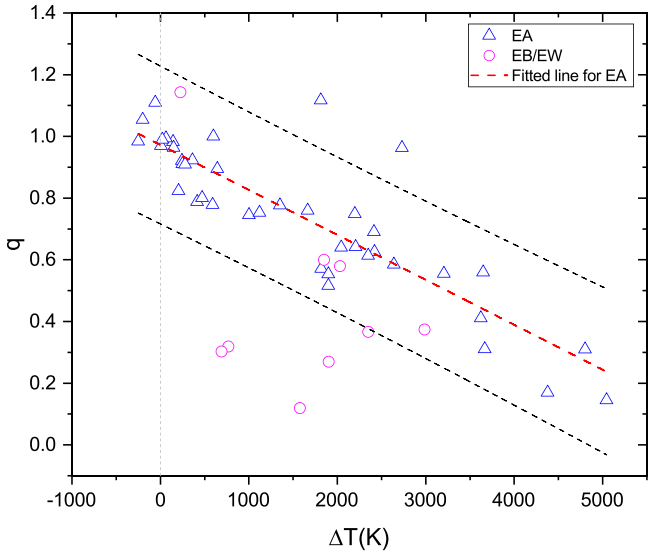

Figure 23. The relation of the temperature difference to the mass ratio for the eclipsing Am binaries.

relations of the main sequence quite well. For the systems with $M > 0.81$ M$_\odot$, there are good positive relations in the mass-radius distribution, the mass-luminosity distribution, and the mass-temperature distribution as follows:

$$\log L = 3.340(\pm 0.242) \times \log M + 0.250(\pm 0.061) \quad (11)$$

$$\log R = 0.754(\pm 0.121) \times \log M + 0.144(\pm 0.032) \quad (12)$$

$$\log T = 0.545(\pm 0.045) \times \log M + 3.738(\pm 0.012) \quad (13)$$

Meanwhile, some secondary components with $M < 0.81$ M$_\odot$ (i.e. $\log M < -0.09$ M$_\odot$ in the figure) show quite a dispersion distribution, indicating that they have evolved away from the main sequence. The components are the secondary ones of the following binaries: EW type binaries,V2364 Cyg, V1073 Cyg; EB type binaries, TYC 6408-989-1, GW Gem, V404 Aur, V2787 Ori; EA type, TX Ari, S Vel, RX Gem. Such components may have a higher evolutionary stage than their primary stars. One can see from the Fig. 21, these components appear hotter, larger, and brighter than the main-sequence stars with the same mass, consistent with the original theory of Am phenomenon (Fowler et al. 1965). According to the masses of the secondary components, the predicted main sequence radii (labeled as R_2_MS) were obtained using the empirical relationships of main sequence stars of Eker et al. (2018). The (R_2/R_2_MS)-Period distribution of the secondary components of eclipsing Am binaries is presented in Fig. 22. Some secondaries of semi-detached systems with short periods have evolved, leading to an expansion in their radius. They may has evolved through the giant phase, stripping away most of the hydrogen shell and exposing the stellar core, causing it become hotter and brighter. As a result, their location on the HR diagram will be near or within the main sequence region. The companions of Am stars often show signs of evolution and a history of mass transfer. This has led to the suggestion that the accretion processes, such as mass transfer, may be crucial for the formation of Am peculiarity in binary systems. When mass is transferred from the evolved component of Am type eclipsing binaries, it can cause chemical elements in the atmosphere of the companion stars to recombine. This may result in the presence of chemical anomalies in the composition, as observed in the well-studied marginal

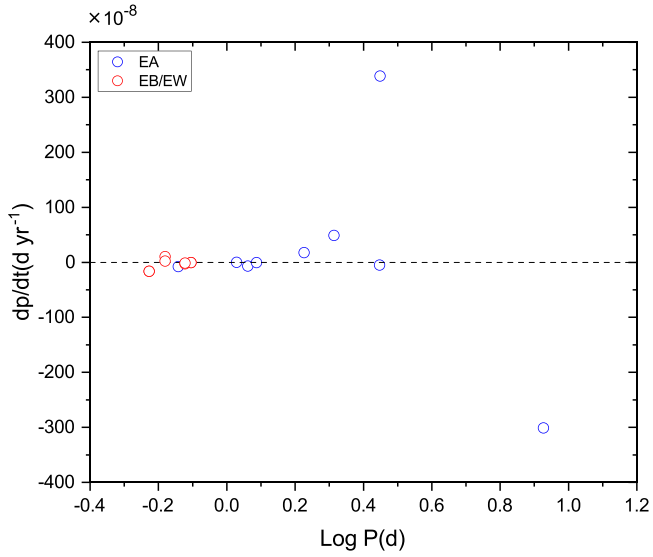

Figure 24. The distributions and relations of dp/dt versus log P.

contact binary V1073 Cyg (Tian et al. 2018), V2787 Ori (Tian et al. 2019), TYC 6408-989-1 (Tian 2021), which are lying on the thermal relaxation oscillation state.

The relation of the temperature difference $\Delta T = T_1 - T_2$ to the mass ratio q of the systems is shown in Fig. 23. The ΔT-q relation of the EA type systems shows a well-linear relation:

$$q = -1.457(\pm 0.134) \times 10^{-4} \times \Delta T + 0.972(\pm 0.029) \quad (14)$$

which was shown with the red dashed line in Fig. 23, with the thin black dash lines representing the edges of the strip defined by the 5% and 95% percentiles of q for each ΔT bin. There are only very few systems with ΔT<0 K. The mass ratio has a negative correlation with the temperature difference, which means that when the components have nearly the same temperature, they will have nearly the same mass. We noticed that there are some EA type system with quite large temperature differences, up to 5 000 K.

https://doi.org/10.1017/pasa.2024.115 Published online by Cambridge University Press

The rate of period change dp/dt is crucial for investigating the orbital evolution of close binaries. Unfortunately, the available information on period changes in these systems is severely limited. Only 12 systems have been thoroughly studied concerning period change. The relationship between period change and the period is illustrated in Fig. 24. The period change of EA type systems shows a wide range. However, more research is needed to obtain period change information for additional systems in the future.

It is generally accepted that the largest equatorial rotational velocity of Am stars is about 120 km s^{-1} (Abt & Moyd 1973; Abt 2000). It is assumed that the components are likely to be rotating synchronously in a circular orbit for short-period binary systems, and the possible slight ellipticity of the long-period systems has little influence. Thus, for all the system with a assuming circle orbit, the equatorial rotational velocities were estimated using the same equation mentioned above: $v = 50.6(R/R_{\odot})/(P/d)$ km s^{-1}(Carquillat & Prieur 2007). Then the projected rotational velocities can be obtained based on the photometric solution and are listed in Table 8. The components of most eclipsing Am binaries in Table 8 exhibit slow rotation, with the rotational velocities less than 120 km s^{-1}. There are certain primary components with a projected rotational velocity of more than 120 km s^{-1}, such as TYC 6408-989-1($v_1 \sin i = 159$ km s^{-1}), V2364 Cyg ($v_1 \sin i = 178$ km s^{-1}), GW Gem ($v_1 \sin i = 122$ km s^{-1}), EU Peg ($v_1 \sin i = 148$ km s^{-1}), V404 Aur ($v_1 \sin i = 130$ km s^{-1}), V1073 Cyg ($v_1 \sin i = 154$ km s^{-1}), and V2787 Ori ($v_1 \sin i = 152$ km s^{-1}. All of targets are short-period systems with periods of less than 1 day. The targets with a short period of less than 1.2 days or with large rotational velocity are important to explore the real relationship between the Am peculiarity and the stellar rotation of Am stars.

Acknowledgements. This work is supported by the National Natural Science Foundation of China (Grant Nos. 12103030, 12303038), the Natural Science of Shandong Province (Grant No. ZR2021QA082), the Natural Science Foundation of Xinjiang Uygur Autonomous Rejion (Grant No. 2022DO1A164), the Joint Research Found (Grant No. U1831109) in Astronomy under cooperative agreement between the National Science Foundation of China (NSFC) and Chinese Academy of Sciences (CAS), and the Young Talent Project of 'Yunnan Revitalization Talent Support Program' and CAS 'Light of West China' Program. This work was partly supported by the Research Fund of Key Laboratory of Aircraft Environment Control and Life Support, MIIT, Nanjing University of Aeronautics and Astronautics(Grant No. KLAECLS minus;E minus;202203).

CCD photometric observations of the system were obtained with the 80 and 85 cm telescope at Xinglong station of National Astronomical Observatory. The spectra observation were obtained with the 2.16 m telescope at Xinglong station of National Astronomical Observatory. We acknowledge the support of the staff of the Xinglong 2.16 m, 85 cm and 80 cm telescope. This work was partially supported by the Open Project Program of the Key Laboratory of Optical Astronomy, National Astronomical Observatories, Chinese Academy of Sciences.

References

Abt, H. A. 1961, ApJS, 6, 37
Abt, H. A. 1965, ApJS, 11, 429
Abt, H. A. 2000, ApJ, 544, 933
Abt, H. A., & Moyd, K. I. 1973, ApJ, 182, 809
Agerer, F., & Hubscher, J. 1999, IBVS, 4711, 1
Agerer, F., & Hubscher, J. 2000, IBVS, 4912, 1
Agerer, F., & Huebscher, J. 1997, IBVA, 4472, 1
Agerer, F., & Huebscher, J. 1998, IBVS, 4562, 1
Agnesoni, C., et al. 1978, BBSAG, 36, 1
Agnesoni, C., et al. 1980, BBSAG, 46, 1
Andersen, J., & Vaz, L. P. R. 1984, A&A, 130, 102
Andrakakou, M., et al. 1983, BBSAG, 66, 1
Ažusienis, A., & Straižys, V. 1969, SvA, 13, 316
Bakış, V., et al. 2022, doi: 10.1016/j.newast.2021.101754, 93, 101754
Bessell, M. S. 1983, PASP, 95, 480
Brat, L., et al. 2009, OEJV, 107, 1
Brat, L., et al. 2011, OEJV, 137, 1
Bressan, A., Marigo, P., Girardi, L., Salasnich, B., Dal Cero, C., Rubele, S., & Nanni, A. 2012, MNRAS, 427, 127
Broglia, P., & Conconi, P. 1981, A&AS, 46, 185
Budaj, J. 1996, A&A, 313, 523
Bulut, A. 2022, RAA, 22, 115006
Bulut, I., et al. 2005, PASJ, 57, 335
Carnevali, P., et al. 1975, BBSAG, 19, 1
Carquillat, J. M., Ginestet, N., Prieur, J. L., & Debernardi, Y. 2003, MNRAS, 346, 555
Carquillat, J. M., & Prieur, J. L. 2007, MNRAS, 380, 1064
Chabrier, G. 2001, ApJ, 554, 1274
Chaplin, G. B. 2019, 47, 222
Chen, Y., Bressan, A., Girardi, L., Marigo, P., Kong, X., & Lanza, A. 2015, MNRAS, 452, 1068
Chen, Y., Girardi, L., Bressan, A., Marigo, P., Barbieri, M., & Kong, X. 2014, MNRAS, 444, 2525
Conti, P. S. 1970, PASP, 82, 781
Değirmenci, Ö. L., Gülmen, Ö., Sezer, C., Ibanoğlu, C., & Çakrl, Ö. 2003, A&A, 409, 959
Diethelm, R. 2005, IBVS, 5653, 1
Diethelm, R. 2009, IBVS, 5871, 1
Diethelm, R. 2011, IBVS, 5960, 1
Diethelm, R., Germann, R., Locher, K., Peter, H., Wittwer, H., Forster, S., & Morger, P. 1974, BBSAG, 13, 1
Diethelm, R., et al. 1983a, BBSAG, 64, 1
Diethelm, R., et al., 1983b, BBSAG, 65, 1
Doğru, D., Erdem, A., Doğru, S. S., & Zola, S. 2009, MNRAS, 397, 1647
Dvorak, S. W. 2003, IBVS, 5378, 1
Eker, Z., et al. 2018, MNRAS, 479, 5491
Ekmekçi, F., et al. 2012, doi: 10.1016/j.newast.2012.03.001, 17, 603
Fan, Z., et al. 2016, PASP, 128, 115005
Fowler, W. A., Burbidge, E. M., Burbidge, G. R., & Hoyle, F. 1965, ApJ, 142, 423
Gallenne, A., et al. 2019, A&A, 632, A31
Garca, J. M., Giménez, A., & Claret, A. 1990, 21, 382
Glazunova, L. V. 2011, AstL, 37, 414
Glazunova, L. V., Yushchenko, A. V., Tsymbal, V. V., Mkrtichian, D. E., Lee, J. J., Kang, Y. W., Valyavin, G. G., & Lee, B. C. 2008, AJ, 136, 1736
Graczyk, D., et al. 2022, A&A, 666, A128
Guarro-Flo, J., Garcia-Melendo, E., Juan-Samso, J., Vidal-Sainz, J., & Poch-Creixell, J. 1995, IBVS, 4245, 1
Hambsch, F.-J., Lampens, P., van Cauteren, P., Kleidis, S., Robertson, C. W., Krajci, T., & Wils, P. 2010, IBVS, 5949, 1
Hauck, N. 2011, BAVSR, 60, 153
Hilditch, R. W., Collier Cameron, A., Hill, G., Bell, S. A., & Harries, T. J. 1997, MNRAS, 291, 749
Honková, K., et al. 2014, OEJV, 165, 1
Hoňková, K., et al. 2013, OEJV, 160, 1
Hubrig, S., González, J., & Schöller, M. 2010, in Astronomical Society of the Pacific Conference Series, Vol. 435, Binaries - Key to Comprehension of the Universe, ed. A. Prša, & M. Zejda, 257
Hubscher, J. 2007, IBVS, 5802, 1
Hubscher, J. 2014, IBVS, 6118, 1
Hubscher, J. 2015, IBVS, 6152, 1
Hubscher, J. 2016, IBVS, 6157, 1
Hubscher, J. 2017, IBVS, 6196, 1
Hubscher, J., & Lehmann, P. B. 2015, IBVS, 6149, 1
Hubscher, J., Lehmann, P. B., & Walter, F. 2012, IBVS, 6010, 1
Hubscher, J., Steinbach, H.-M., & Walter, F. 2009, IBVS, 5874, 1
Ibanoğlu, C., et al. 2008, MNRAS, 390, 958

Ismailov, N. Z. 1987, Afz, 27, 471
Jableka, D., Zola, S., Zakrzewski, B., Szymanski, T., Kuzmicz, A., de Villiers, S. N., Zejda, M., & Koziel-Wierzbowska, D. 2012, AASP, 2, 128
Juryšek, J., et al. 2017, OEJVS, 179, 1
Kahraman Aliçavuş, F., & Aliçavuş, F. 2020, RAA, 20, 150
Khaliullin, K. F., & Khaliullina, A. I. 2002, ARep, 46, 119
Khaliullina, A. I. 2021, ARep, 65, 569
Kippenhahn, R. 1953, AN, 281, 153
Koleva, M., Prugniel, P., Bouchard, A., & Wu, Y. 2009, A&A, 501, 1269
Kurtz, D. W., et al. 2020, MNRAS, 494, 5118
Lacy, C. H. S., Vaz, L. P. R., Claret, A., & Sabby, J. A. 2004, AJ, 128, 1324
Lee, J. W., Kim, S.-L., Lee, C.-U., Kim, H.-I., Park, J.-H., Park, S.-R., & Koch, R. H. 2009, PASP, 121, 104
Lehký, M. H. K., et al. 2021, OEJVS, 211, 1
Li, L., Zhang, F., Han, Z., Jiang, D., & Jiang, T. 2008, MNRAS, 387, 97
Liakos, A., & Niarchos, P. 2012, Ap&SS, 340, 281
Liao, W.-P., & Qian, S.-B. 2010, PASJ, 62, 1109
Liao, W.-P., Qian, S.-B., Zejda, M., Zhu, L.-Y., & Li, L.-J. 2016, RAA, 16, 94
Liao, W. P., Qian, S. B., Li, L. J., Zhou, X., Zhao, E. G., & Zhang, J. 2017, PASP, 129, 034201
Liao, W. P., Qian, S. B., & Liu, N. P. 2012, AJ, 144, 178
Liao, W. P., Qian, S. B., & Sarotsakulchai, T. 2019, AJ, 157, 207
Liao, W. P., & Sarotsakulchai, T. 2019, PASP, 131, 014202
Lightkurve Collaboration et al. 2018, Lightkurve: Kepler and TESS time series analysis in Python, Astrophysics Source Code Library, record ascl:1812.013
Linnell, A. P., Hubeny, I., & Lacy, C. H. S. 1995, in American Astronomical Society Meeting Abstracts, 60.06
Liu, Q., & Yang, Y. 1999, in Observational Astrophysics in Asia and its Future, Vol. 4, P. S. Chen, 377
Locher, K. 1979, BBSAG, 43, 4
Michaels, E. J. 2017, 45, 43
Milone, E. F. 1969, Commmunications of the Konkoly Observatory Hungary, 65, 457
Monier, R. 2005, A&A, 442, 563
Monier, R., & Richard, O. 2004, in The A-Star Puzzle, Vol. 224, ed. J. Zverko, J. Ziznovsky, S. J. Adelman, & W. W. Weiss, 209, 10.1017/S1743921304004570
Nelson, R. H. 2001, IBVS, 5040, 1
Nelson, R. H. 2003, IBVS, 5371, 1
Nelson, R. H. 2007, IBVS, 5760, 1
Nelson, R. H. 2008, IBVS, 5820, 1
Nelson, R. H. 2009, IBVS, 5875, 1
Nelson, R. H., Terrell, D., & Gross, J. 2006, IBVS, 5715, 1
Ogloza, W., Niewiadomski, W., Barnacka, A., Biskup, M., Malek, K., & Sokolowski, M. 2008, IBVS, 5843, 1
Okazaki, A., Yamasaki, A., Nurwendaya, C., & Malasan, H. L. 1985, PASP, 97, 62
Olson, E. C., & Etzel, P. B. 2015, AJ, 149, 125
Pavlovski, K., Southworth, J., Kolbas, V., & Smalley, B. 2014, MNRAS, 438, 590
Polubek, G. 2001, OAP, 14, 65
Popper, D. M. 1981, ApJ, 244, 541
Popper, D. M. 1984, AJ, 10.1086/113601, 89, 1057
Popper, D. M. 1988, AJ, 10.1086/114864, 96, 1040
Popper, D. M., Andersen, J., Clausen, J. V., & Nordstrom, B. 1985, AJ, 90, 1324
Pribulla, T., et al. 2006, AJ, 132, 769
Prugniel, P., & Soubiran, C. 2001, A&A, 369, 1048
Qian, S. 2001, AJ, 121, 1614
Qian, S. 2002, Ap&SS, 282, 399
Qian, S. 2003, PASJ, 55, 289
Qian, S. B., Liu, N. P., Liao, W. P., He, J. J., Liu, L., Zhu, L. Y., Wang, J. J., & Zhao, E. G. 2013, AJ, 146, 38
Qian, S. B., & Zhu, L. Y. 2002, ApJ, 568, 1004
Qian, S. B., et al. 2014, ApJS, 212, 4
Rachkovskaia, T. M. 1985, IzKry, 70, 134
Ricker, G. R., et al. 2014, in Society of Photo-Optical Instrumentation Engineers (SPIE) Conference Series, Vol. 9143, Space Telescopes and Instrumentation 2014: Optical, Infrared, and Millimeter Wave, ed. M. J. Oschmann Jacobus, M. Clampin, G. G. Fazio, & H. A. MacEwen, 914320 (arXiv:1406.0151), doi: 10.1117/12.2063489
Roman, N. G., Morgan, W. W., & Eggen, O. J. 1948, ApJ, 107, 107
Ruciński, S. M. 1969, AcA, 19, 245
Rudiger, G. 1983, in Magnetic and Variable Stars, 194
Samus', N. N., Kazarovets, E. V., Durlevich, O. V., Kireeva, N. N., & Pastukhova, E. N. 2017, ARep, 61, 80
Smalley, B., et al. 2014, A&A, 564, A69
Southworth, J. 2021, Obs, 141, 282
Southworth, J., & Clausen, J. V. 2006, arXiv e-prints, pp astro–ph/0608016
Southworth, J., Pavlovski, K., Tamajo, E., Smalley, B., West, R. G., & Anderson, D. R. 2011, MNRAS, 414, 3740
Southworth, J., Smalley, B., Maxted, P. F. L., Claret, A., & Etzel, P. B. 2005, MNRAS, 363, 529
Soydugan, F., Erdem, A., Doğru, S. S., Aliçavuş, F., Soydugan, E., Çiçek, C., & Demircan, O. 2011, doi: 10.1016/j.newast.2010.11.006, 16, 253
Sun, W., Chen, X., Deng, L., & de Grijs, R. 2020, ApJS, 247, 50
Sürgit, D., Erdem, A., Engelbrecht, C. A., van Heerden, H. P., & Manick, R. 2017, doi: 10.1016/j.newast.2017.01.013, 54, 109
Takeda, Y., Han, I., Kang, D.-I., Lee, B.-C., & Kim, K.-M. 2019, MNRAS, 485, 1067
Tang, J., Bressan, A., Rosenfield, P., Slemer, A., Marigo, P., Girardi, L., & Bianchi, L. 2014, MNRAS, 445, 4287
Tian, X.-M. 2021, RAA, 21, 062
Tian, X.-M., & Zhu, L.-Y. 2019, PASJ, 71, 66
Tian, X.-M., Zhu, L.-Y., Qian, S.-B., Li, L.-J., & Jiang, L.-Q. 2018, RAA, 18, 020
Tian, X.-m., Wang, Z.-h., Zhu, L.-y., & Yang, X.-L. 2023, ApJS, 266, 14
Tian, X.-m., Zhu, L.-y., & Wang, Z.-h. 2019, PASP, 131, 084203
Titus, J., & Morgan, W. W. 1940, ApJ, 92, 256
Tkachenko, A., Lehmann, H., & Mkrtichian, D. 2010, AJ, 139, 1327
Torres, G., et al. 1999, AJ, 118, 1831
Torres, G., Andersen, J., Nordström, B., & Latham, D. W. 2000, AJ, 119, 1942
Tout, C. A., & Eggleton, P. P. 1988, MNRAS, 231, 823
Tucker, R. S., Sowell, J. R., Williamon, R. M., & Coughlin, J. L. 2009, AJ, 137, 2949
Ulaş, B., Ulusoy, C., Erkan, N., Madiba, M., & Matsete, M. 2022, Ap&SS, 367, 22
van Hamme, W. 1993, AJ, 106, 2096
van't Veer, F. 1996, in Astronomical Society of the Pacific Conference Series, Vol. 90, The Origins, Evolution, and Destinies of Binary Stars in Clusters, ed. E. F. Milone, & J. C. Mermilliod, 280
Vivekananda Rao, P., Sarma, M. B. K., & Prakash Rao, B. V. N. S. 1994, JApA, 15, 165
Wilson, R. E. 1990, ApJ, 356, 613
Wilson, R. E. 2012, AJ, 144, 73
Wilson, R. E., & Devinney, E. J. 1971, ApJ, 166, 605
Yakut, K., et al. 2009, A&A, 503, 165
Yang, Y., & Wei, J. 2011, in Astronomical Society of the Pacific Conference Series, Vol. 451, 9th Pacific Rim Conference on Stellar Astrophysics, ed. S. Qain, K. Leung, L. Zhu, & S. Kwok, 39
Yang, Y., Yuan, H., Dai, H., & Zhang, X. 2018, PASJ, 70, 24
Yuan, H.-Y., Jiang, L.-Q., Dai, H.-F., Wang, S., & Yang, Y.-G. 2020, RAA, 20, 203
Yücel, G., & Bakış, V. 2022, MNRAS, 514, 34
Zakirov, M. M. 1998, AstL, 24, 808
Zasche, P. 2015, doi: 10.1016/j.newast.2014.07.008, 34, 253
Zasche, P. 2017, doi: 10.1016/j.newast.2016.12.002, 53, 53
Zasche, P., Svoboda, P., & Šlechta, M. 2012, MNRAS, 421, 1196
Zasche, P., Uhlař, R., Svoboda, P., Cagaš, P., & Mašek, M. 2020, A&A, 643, A130
Zhang, J., Qian, S.-B., Wu, Y., & Zhou, X. 2019, ApJS, 244, 43
Zhu, L. Y., Qian, S. B., Zola, S., & Kreiner, J. M. 2009, AJ, 137, 3574
Zhu, L. Y., Zejda, M., Mikulášek, Z., Liška, J., Qian, S. B., & de Villiers, S. N. 2012, AJ, 144, 37
Zhu, L.-Y., Tian, X.-M., Zhou, X., Li, L.-J., & Wang, Z.-H. 2019, RAA, 19, 094
Zverko, J., Ziznovsky, J., & Khokhlova, V. L. 1997, CoSka, 27, 41

https://doi.org/10.1017/pasa.2024.115 Published online by Cambridge University Press

A. Light Minimum for V404 Aur

Table A1. All available Light Minimum for V404 Aur.

HJD (2400000+)	Error	Meth.	*E*	*O* − *C* (d)	Ref.	HJD (2400000+)	Error	Meth.	E	*O* − *C* (d)	Ref.
38496.32800		pg	−2 8436	−0.0484372	*	56241.32539	0.00180	V	−4 911.5	0.01162895	(15)
38849.35200		pg	−27 968	−0.0449336	*	56241.32729	0.00190	I	−4 911.5	0.01352895	(15)
38852.36200		pg	−27 964	−0.0522028	*	56291.47996	0.00030	I	−4 845	0.0040985	(15)
39029.61600		pg	−27 729	−0.0627683	*	56291.48099	0.00031	R	−4 845	0.0051285	(16)
39057.55100		pg	−27 692	−0.0375084	*	56291.48107	0.00020	R	−4 845	0.0052085	(15)
39917.49300		pg	−26 552	−0.0172304	*	56291.48149	0.00030	V	−4 845	0.0056285	(15)
41364.29300		pg	−24 634	0.0021882	*	56691.26890	0.00020	ccd	−4 315	0.0048695	(17)
41385.36900		pg	−24 606	−0.0426962	*	57073.33294	0.00070	I	−3 808.5	0.00719705	(18)
41592.45000		pg	−24 331.5	−0.02179505	*	57073.33385	0.00130	V	−3 808.5	0.00810705	(18)
41600.39300		pg	−24 321	0.0008733	*	57073.33413	0.00070	R	−3 808.5	0.00838705	(18)
41677.30800		pg	−24 219	−0.0244913	*	57364.49970	0.00590	−I	−3 422.5	0.00747925	(19)
41680.33400		pg	−24 215	−0.0157605	*	57631.52861	0.00380	R	−3 068.5	0.00806505	(17)
41689.37900		pg	−24 203	−0.0225681	*	57631.52950	0.00310	I	−3 068.5	0.00895505	(18)
41741.42400		pg	−24 134	−0.0254618	*	57631.53049	0.00090	V	−3 068.5	0.00994505	(18)
41766.32100		pg	−24 101	−0.0209327	*	57722.42004	0.00020	V	−2 948	0.0042604	(20)
42395.42000		pg	−23 267	−0.0225609	*	57722.42039	0.00020	R	−2 948	0.0046104	(20)
43571.39000		pg	−21 708	−0.0332316	*	57722.42135	0.00020	I	−2 948	0.0055704	(20)
43605.32300		pg	−21 663	−0.044510101	*	58817.68580	0.00150	ccd	−1 496	0.00130201	This study*
43847.49500		pg	−21 342	−0.0083634	*	58818.06389	0.00068	ccd	−1 495.5	0.00223257	This study*
43850.51200		pg	−21 338	−0.0086326	*	58818.44248	0.00108	ccd	−1 495	0.00366432	This study*
43933.47000		pg	−21 228	−0.0255356	*	58818.82170	0.00130	ccd	−1 494.5	0.00572575	This study*
43955.35600		pg	−21 199	−0.0147373	*	58819.19600	0.00133	ccd	−1 494	0.00286765	This study*
44252.54000		pg	−20 805	−0.0317535	*	58819.57444	0.00126	ccd	−1 493.5	0.00414877	This study*
44289.52100		pg	−20 756	−0.0123012	*	58819.95176	0.00151	ccd	−1 493	0.00430944	This study*
44314.38700		pg	−20 723	−0.0387721	*	58820.32957	0.00092	ccd	−1 492.5	0.00496084	This study*
44692.32100		pg	−20 222	−0.0177394	*	58820.70512	0.00654	ccd	−1 492	0.0033527	This study*
44701.36900		pg	−20 210	−0.021547	*	58821.08381	0.00647	ccd	−1 491.5	0.00488373	This study*
46491.38000		pg	−17 837	−0.0054999	*	58821.45831	0.00407	ccd	−1 491	0.00222561	This study*
46881.37600		pg	−17 320	0.008456	*	58821.84010	0.00329	ccd	−1 490.5	0.00685637	This study*
47974.38500		pg	−15 871	0.011688299	*	58822.21404	0.00108	ccd	−1 490	0.00363794	This study*
49825.47600	0.00100	ccd	−13 417	0.0080341	(1)	58822.59179	0.00085	ccd	−1 489.5	0.00423001	This study*
50096.26800		ccd	−13 058	0.0001234	(2)	58822.96717	0.00129	ccd	−1 489	0.00245027	This study*
50101.54740		ccd	−13 051	−0.0006977	(2)	58823.34709	0.00204	ccd	−1 488.5	0.0052126	This study*
50151.33350		ccd	−12 985	0.0004605	(2)	58823.72277	0.00167	ccd	−1 488	0.0037337	This study*
50446.27290	0.00090	ccd	−12 594	0.0017962	(3)	58824.10021	0.00098	ccd	−1 487.5	0.00401538	This study*
50706.51200	0.00180	ccd	−12 249	0.0014277	(4)	58824.47641	0.00167	ccd	−1 487	0.00305614	This study*
50749.50730	0.00030	ccd	−12 192	0.0006416	(4)	58824.85558	0.00118	ccd	−1 486.5	0.0050681	This study*
50799.29040	0.00070	ccd	−12 126	−0.001200201	(4)	58825.23236	0.00114	ccd	−1 486	0.00468868	This study*
51189.27310	0.00080	ccd	−11 609	−0.0005443	(5)	58825.61358	0.00306	ccd	−1 485.5	0.00875052	This study*
51934.54350		ccd	−10 621	0.0043633	*	58825.98667	0.00201	ccd	−1 485	0.00468191	This study*
52276.24800		ccd	−10 168	0.0031264	*	58826.36479	0.00113	ccd	−1 484.5	0.005642639	This study*
52337.35020		ccd	−10 087	0.0056251	*	58826.73750	0.00209	ccd	−1 484	0.00119427	This study*

https://doi.org/10.1017/pasa.2024.115 Published online by Cambridge University Press

Table A1. (Continued)

HJD (2400000+)	Error	Meth.	*E*	*O* − *C* (d)	Ref.	HJD (2400000+)	Error	Meth.	E	*O* − *C* (d)	Ref.
53381.32120	0.00080	V	−8 703	0.0014819	(6)	58827.11788	0.00074	ccd	−1 483.5	0.00441554	This study*
53738.86790	0.0001	R	−8 229	0.0017817	(7)	58827.49440	0.00108	ccd	−1 483	0.00377751	This study*
53814.67480	0.0005	R	−8 128.5	−0.00020695	(7)	58830.51120	0.00155	ccd	−1 479	0.00330808	This study*
53991.56340	0.00030	−Ir	−7 894	0.0009862	(8)	58830.88792	0.00158	ccd	−1 478.5	0.00286969	This study*
54115.27220	0.00020	−Ir	−7 730	0.001749	(9)	58831.26662	0.00116	ccd	−1 478	0.00441051	This study*
54116.41210	0.00220	−Ir	−7 728.5	0.01017305	(8)	58831.64354	0.00115	ccd	−1 477.5	0.00417218	This study*
54164.30260	0.00040	−Ir	−7 665	0.0015245	(9)	58832.02286	0.00405	ccd	−1 477	0.00633332	This study*
54171.48470	0.00320	−Ir	−7 655.5	0.01761015	(8)	58832.39813	0.00053	ccd	−1 476.5	0.00444539	This study*
54176.37070	0.00090	−Ir	−7 649	0.0005477	(9)	58832.77166	0.00444	ccd	−1 476	0.00081644	This study*
54398.89610	0.00020	R	−7 354	0.0023442	(10)	58833.15049	0.00141	ccd	−1 475.5	0.0024877	This study*
54794.91110	0.00040	V	−6 829	0.0007617	(11)	58833.52848	0.00579	ccd	−1 475	0.00331848	This study*
55480.58830	0.0001	ccd	−5 920	0.003536	(12)	58834.66230	0.00132	ccd	−1 473.5	0.00566327	This study*
55482.47744	0.00100	R	−5 917.5	0.00688275	(13)	58835.03471	0.00326	ccd	−1 473	0.00091451	This study*
55482.47755	0.00190	V	−5 917.5	0.00699275	(13)	58835.40611	0.00242	ccd	−1 472.5	−0.00484483	This study*
55482.47777	0.00080	I	−5 917.5	0.00721275	(13)	58835.79358	0.00335	ccd	−1 472	0.00546646	This study*
55528.86450	0.00030	V	−5 856	0.0034288	(14)	58836.17223	0.01400	ccd	−1 471.5	0.00695873	This study*
55894.33619	0.00080	R	−5 371.5	0.00838695	(15)	58836.54724	0.00361	ccd	−1 471	0.00480933	This study*
55894.33629	0.00070	I	−5 371.5	0.00848695	(15)	58836.92211	0.00140	ccd	−1 470.5	0.00252092	This study*
55894.33680	0.01000	V	−5 371.5	0.00899695	(15)	58837.29903	0.00241	ccd	−1 470	0.00228236	This study*
55960.33552	0.00030	V	−5 284	0.0049532	(15)	58837.67628	0.00062	ccd	−1 469.5	0.00237358	This study*
55960.33553	0.00030	R	−5 284	0.0049632	(15)	58838.05564	0.00151	ccd	−1 469	0.00457483	This study*
55960.33611	0.00060	I	−5 284	0.0055432	(15)	58838.43258	0.00091	ccd	−1 468.5	0.00435681	This study*
56241.32299	0.00160	R	−4 911.5	0.009228949	(15)	58839.19095	0.00164	ccd	−1 467.5	0.00840918	This study*
58839.94057	0.00173	ccd	−1 466.5	0.00371156	This study*	59935.58255	0.00027	ccd	−14	−0.00018498	This study*
58840.31778	0.00097	ccd	−1 466	0.00376386	This study*	59935.96137	0.00066	ccd	−13.5	0.00147647	This study*
58840.69423	0.00089	ccd	−1 465.5	0.00305435	This study*	59936.33762	0.00026	ccd	−13	0.00056711	This study*
59913.70813	0.00037	ccd	−43	0.00059493	This study*	59946.14318	0.00029	BVRcIc	0	0	This study
59914.08894	0.00069	ccd	−42.5	0.00424667	This study*	59947.27615	0.00034	BVRcIc	1.5	0.00149405	This study
59914.46294	0.00029	ccd	−42	0.001087809	This study*	60290.11315	0.00045	ccd	456	0.00127903	This study*
59914.84137	0.00055	ccd	−41.5	0.00235945	This study*	60290.49045	0.00065	ccd	456.5	0.00142051	This study*
59915.21636	0.00028	ccd	−41	0.00019092	This study*	60290.86559	0.00022	ccd	457	−0.00059794	This study*
59915.59283	0.00063	ccd	−40.5	−0.0004975	This study*	60291.24393	0.00060	ccd	457.5	0.00058363	This study*
59915.97115	0.00029	ccd	−40	0.00066349	This study*	60291.62094	0.00023	ccd	458	0.00043506	This study*
59916.34738	0.00082	ccd	−39.5	−0.00026497	This study*	60291.99708	0.00054	ccd	458.5	−0.0005841	This study*
59917.10242	0.00066	ccd	−38.5	0.00045748	This study*	60292.75317	0.00055	ccd	459.5	0.00118944	This study*
59917.47953	0.00031	ccd	−38	0.00040923	This study*	60293.12876	0.00022	ccd	460	−0.00037907	This study*
59917.85838	0.00065	ccd	−37.5	0.00210035	This study*	60293.50536	0.00059	ccd	460.5	−0.00093848	This study*
59918.23377	0.00029	ccd	−37	0.00033166	This study*	60293.88254	0.00024	ccd	461	−0.00091716	This study*
59918.61282	0.00057	ccd	−36.5	0.00222264	This study*	60294.26107	0.00058	ccd	461.5	0.00045468	This study*
59918.98785	0.00028	ccd	−36	9.46503E-05	This study*	60294.63700	0.00024	ccd	462	−0.00077446	This study*
59919.36706	0.00065	ccd	−35.5	0.00214602	This study*	60295.01248	0.00057	ccd	462.5	−0.00245291	This study*
59919.74215	0.00028	ccd	−35	7.66898E-05	This study*	60295.39089	0.00024	ccd	463	−0.00120103	This study*
59920.12208	0.00063	ccd	−34.5	0.0028487	This study*	60295.76895	0.00057	ccd	463.5	−0.00030004	This study*
59920.49680	0.00027	ccd	−34	0.00040966	This study*	60296.14608	0.00023	ccd	464	−0.00032874	This study*
59920.87527	0.00057	ccd	−33.5	0.00172165	This study*	60296.52155	0.00058	ccd	464.5	−0.00201736	This study*

https://doi.org/10.1017/pasa.2024.115 Published online by Cambridge University Press

Table A1. (Continued)

HJD (2400000+)	Error	Meth.	E	$O-C$ (d)	Ref.	HJD (2400000+)	Error	Meth.	E	$O-C$ (d)	Ref.
59921.25103	0.00030	ccd	−33	0.00032271	This study*	60296.89975	0.00024	ccd	465	−0.00097595	This study*
59921.62940	0.00069	ccd	−32.5	0.00153359	This study*	60297.27979	0.00060	ccd	465.5	0.00190556	This study*
59922.00510	0.00035	ccd	−32	7.67498E-05	This study*	60297.65415	0.00022	ccd	466	−0.00089376	This study*
59922.38506	0.00068	ccd	−31.5	0.00287706	This study*	60298.03176	0.00053	ccd	466.5	−0.00044213	This study*
59922.76032	0.00029	ccd	−31	0.00097832	This study*	60298.40846	0.00024	ccd	467	−0.00090043	This study*
59928.04050	0.00035	ccd	−24	0.00093787	This study*	60298.78276	0.00063	ccd	467.5	−0.00375948	This study*
59928.41981	0.00069	ccd	−23.5	0.00308902	This study*	60306.33356	0.00063	ccd	477.5	0.003868	This study*
59928.79380	0.00027	ccd	−23	−7.96001E-05	This study*	60306.70626	0.00023	ccd	478	−0.00059082	This study*
59929.17190	0.00056	ccd	−22.5	0.00086161	This study*	60307.08355	0.00052	ccd	478.5	−0.00045846	This study*
59929.54821	0.00028	ccd	−22	1.32099E-05	This study*	60307.46076	0.00023	ccd	479	−0.00040737	This study*
59929.92684	0.00063	ccd	−21.5	0.00148398	This study*	60307.83783	0.00063	ccd	479.5	−0.00049661	This study*
59930.68136	0.00064	ccd	−20.5	0.00168642	This study*	60308.21511	0.00024	ccd	480	−0.00037536	This study*
59931.05699	0.00028	ccd	−20	0.0001588	This study*	60308.59252	0.00057	ccd	480.5	−0.00012362	This study*
59931.43602	0.00059	ccd	−19.5	0.00202915	This study*	60308.96923	0.00024	ccd	481	−0.00057231	This study*
59931.81158	0.00029	ccd	−19	0.00043047	This study*	60309.34778	0.00053	ccd	481.5	0.00081902	This study*
59932.18984	0.00057	ccd	−18.5	0.001532929	This study*	60309.72349	0.00025	ccd	482	−0.00062897	This study*
59932.56561	0.00026	ccd	−18	0.00014333	This study*	60310.10143	0.00052	ccd	482.5	0.00015196	This study*
59932.94295	0.00067	ccd	−17.5	0.00032516	This study*	60310.47762	0.00023	ccd	483	−0.00081732	This study*
59933.31928	0.00028	ccd	−17	−0.00050363	This study*	60310.85467	0.00055	ccd	483.5	−0.00092573	This study*
59933.69769	0.00060	ccd	−16.5	0.00074842	This study*	60311.23214	0.00024	ccd	484	−0.00061429	This study*
59934.07471	0.00028	ccd	−16	0.000608949	This study*	60311.61153	0.00057	ccd	484.5	0.00161708	This study*
59934.45234	0.00060	ccd	−15.5	0.00108037	This study*	60311.98715	0.00023	ccd	485	7.85599E-05	This study*
59934.82845	0.00029	ccd	−15	3.18796E-05	This study*	60312.36565	0.00050	ccd	485.5	0.00142059	This study*
59935.20529	0.00064	ccd	−14.5	−0.00028649	This study*						

Notes: '*':$O-C$ gateway; 'This study*':light minimums obtained by us based on the TESS light curves; (1) Guarro-Flo et al. (1995) (2) Agerer & Huebscher (1997) (3) Agerer & Huebscher (1998) (4) Agerer & Hubscher (1999) (5) Agerer & Hubscher (2000) (6) Diethelm (2005) (7) Nelson (2007) (8) Hubscher (2007) (9) Hubscher et al. (2009) (10) Nelson (2008) (11) Diethelm (2009) (12) Hubscher et al. (2012) (13) Brat et al. (2011) (14) Diethelm (2011) (15) Hoňková et al. (2013) (16) Honková et al. (2014) (17) Hubscher (2015) (18) Juryšek et al. (2017) (19) Hubscher (2017) (20) Lehký et al. (2021).

https://doi.org/10.1017/pasa.2024.115 Published online by Cambridge University Press

B. Light Minimum for GW GEM

Table B1. All available Light Minimum for GW Gem.

HJD	Error	Meth.	E	$O-C$	Ref.	HJD	Error	Meth.	E	$O-C$	Ref.
(2400000+)				(d)		(2400000+)				(d)	
25645.57200		pg	−52 004	−0.04359	(1)	42858.39200		vis	−25 902	−0.03122	*
25889.54900		pg	−51 634	−0.06087	(1)	42864.32800		vis	−25 893	−0.03021	*
26056.43100		pg	−51 381	−0.01821	(1)	42866.30500		vis	−25 890	−0.03154	*
26352.47100		pg	−50 932	−0.06857	(1)	42885.41600		vis	−25 861	−0.04442	*
26391.43700		pg	−50 873	−0.00977	(2)	42885.43700		vis	−25 861	−0.02342	*
26416.44000		pg	−50 835	−0.06564	(2)	42887.40100		vis	−25 858	−0.03775	*
26416.47100		pg	−50 835	−0.03464	(2)	43103.70200		vis	−25 530	−0.03439	*
26424.35400		pg	−50 823	−0.06497	(2)	43220.43000		vis	−25 353	−0.02798	*
26763.35700		pg	−50 309	−0.01619	(2)	43222.40200		vis	−25 350	−0.03431	*
26767.30100		pg	−50 303	−0.02885	(2)	43496.71600		vis	−24 934	−0.04902	(5)
26769.30800		pg	−50 300	−0.00019	(2)	43514.53440		pe	−24 907	−0.03561	*
26792.36700		pg	−50 265	−0.02173	(2)	43543.55010		pe	−24 863	−0.03544	*
26796.33100		pg	−50 259	−0.01439	(2)	43544.54110		pe	−24 861.5	−0.03361	*
26825.37100		pg	−50 215	0.01007	(2)	43577.51200		pe	−24 811.5	−0.03491	*
26987.52900		pg	−49 969	−0.05515	(1)	43589.37980		pe	−24 793.5	−0.03710	*
27127.31500		pg	−49 757	−0.07129	(2)	43849.53180		pe	−24 399	−0.03577	*
27133.28700		pg	−49 748	−0.03428	(2)	43876.56880		pe	−24 358	−0.03597	*
27154.38700		pg	−49 716	−0.03649	(1)	43905.58450		pe	−24 314	−0.03581	*
27483.43000		pg	−49 217	−0.05605	(2)	43926.35660		pe	−24 282.5	−0.03619	*
28497.66300		pg	−47 679	−0.04794	(1)	43931.30800		vis	−24 275	−0.03062	*
28513.49200		pg	−47 655	−0.04560	(1)	43981.42700		vis	−24 199	−0.02937	(6)
28622.33200		pg	−47 490	−0.01386	(2)	44291.35400		vis	−23 729	−0.04106	(7)
28879.51900		pg	−47 100	−0.01003	(2)	44295.31000		vis	−23 723	−0.04172	(7)
28949.38000		pg	−46 994	−0.05009	(1)	44316.42400		vis	−23 691	−0.02993	*
28949.42400		pg	−46 994	−0.00609	(2)	44643.50200		vis	−23 195	−0.03616	*
28951.35600		pg	−46 991	−0.05243	(2)	45021.37400		vis	−22 622	−0.02558	*
28951.38000		pg	−46 991	−0.02843	(2)	45021.37700		vis	−22 622	−0.02258	*
28978.38600		pg	−46 950	−0.05963	(1)	45052.35900		vis	−22 575	−0.03445	*
29175.58600		pg	−46 651	−0.03339	(2)	45054.34000		vis	−22 572	−0.03178	*
29317.37100		pg	−46 436	−0.02885	(1)	45077.42900		vis	−22 537	−0.02332	*
29317.38800		pg	−46 436	−0.01185	(2)	45079.37500		vis	−22 534	−0.05565	*
29576.51300		pg	−46 043	−0.04835	(1)	45079.39300		vis	−22 534	−0.03765	*
29632.57500		pg	−45 958	−0.03909	(1)	45079.39300		vis	−22 534	−0.03765	*
29687.34100		pg	−45 875	−0.00694	(1)	45352.41500		vis	−22 120	−0.02547	(8)
30750.33200		pg	−44 263	−0.03969	(1)	45383.39900		vis	−22 073	−0.03534	*
30781.34500		pg	−44 216	−0.02056	(1)	45383.41100		vis	−22 073	−0.02334	(9)
31028.63300		pg	−43 841	−0.02407	(1)	45385.38300		vis	−22 070	−0.02967	(9)
31443.44200		pg	−43 212	−0.00535	(1)	45385.38600		vis	−22 070	−0.02667	*
32889.56600		pg	−41 019	−0.04207	*	45387.36600		vis	−22 067	−0.02501	(9)
36226.33900		pg	−35 959	−0.05578	*	45439.45000		vis	−21 988	−0.03708	(10)
36255.38800		pg	−35 915	−0.02231	*	45697.30300		vis	−21 597	−0.02669	*
36257.37100		pg	−35 912	−0.01765	*	45782.36200		vis	−21 468	−0.03597	*

https://doi.org/10.1017/pasa.2024.115 Published online by Cambridge University Press

Table B1. (Continued)

HJD (2400000+)	Error	Meth.	E	$O-C$ (d)	Ref.	HJD (2400000+)	Error	Meth.	E	$O-C$ (d)	Ref.
36317.32700		pg	−35 821	−0.07105	*	45815.32500		vis	−21 418	−0.04517	*
36596.27500		pg	−35 398	−0.06787	*	46113.41400		vis	−20 966	−0.02486	*
39200.43300		pg	−31 449	−0.05428	*	46121.32300		vis	−20 954	−0.02919	*
39206.36200		pg	−31 440	−0.06027	*	46148.35800		vis	−20 913	−0.03140	*
39235.37600		pg	−31 396	−0.06181	*	46171.43900		vis	−20 878	−0.03094	*
39239.32500		pg	−31 390	−0.06947	*	46173.41900		vis	−20 875	−0.02927	*
40290.50100		vis	−29 796	−0.04723	*	46847.36600		vis	−19 853	−0.03405	*
40290.50100		vis	−29 796	−0.04723	*	46914.35000		vis	−19 751.5	0.01638	*
41762.39100		vis	−27 564	−0.03627	*	47176.44300		vis	−19 354	−0.01961	*
41766.35000		vis	−27 558	−0.03393	*	47209.41800		vis	−19 304	−0.01681	*
41795.36700		vis	−27 514	−0.03247	*	47234.46800		vis	−19 266	−0.02569	*
42078.26100		vis	−27 085	−0.03995	(3)	47267.43500		vis	−19 216	−0.03089	*
42132.34200		vis	−27 003	−0.03336	*	47579.35500		vis	−18 743	−0.02790	*
42403.36800		vis	−26 592	−0.03885	(4)	47612.33300		vis	−18 693	−0.02210	*
42403.36900		vis	−26 592	−0.03785	(4)	47922.26400		vis	−18 223	−0.02979	*
42404.68200		vis	−26 590	−0.04373	(4)	47939.42600		vis	−18 197	−0.01334	*
42404.68800		vis	−26 590	−0.03773	(4)	47947.33100		vis	−18 185	−0.02166	*
42408.64800		vis	−26 584	−0.03440	(4)	47969.41600		vis	−18 151.5	−0.02804	*
42426.45500		vis	−26 557	−0.03239	*	47970.41100		vis	−18 150	−0.02220	*
42443.59200		vis	−26 531	−0.04093	*	48001.40500		vis	−18 103	−0.02207	*
42461.40200		vis	−26 504	−0.03592	*	48332.44700		vis	−17 601	−0.02097	*
42525.35700		vis	−26 407	−0.04699	*	48677.33800		vis	−17 078	−0.01919	*
42796.39400		vis	−25 996	−0.04148	*	48708.32800		vis	−17 031	−0.02305	*
48733.38700		vis	−16 993	−0.02293	*	59501.14206	0.000197	ccd	−664.5	0.00057	This study*
49043.32100		vis	−16 523	−0.02761	*	59501.47126	0.000167	ccd	−664	0.00005	This study*
49066.40200		vis	−16 488	−0.02715	*	59501.80170	0.000178	ccd	−663.5	0.00077	This study*
49097.39500		vis	−16 441	−0.02802	*	59502.13080	0.000143	ccd	−663	0.00014	This study*
49384.24400		vis	−16 006	−0.03717	*	59502.46122	0.000145	ccd	−662.5	0.00084	This study*
49769.38600		vis	−15 422	−0.01047	*	59502.79030	0.000109	ccd	−662	0.00020	This study*
49771.34000		vis	−15 419	−0.03480	*	59503.12043	0.000125	ccd	−661.5	0.00061	This study*
50098.43300		vis	−14 923	−0.02603	*	59503.44926	0.000081	ccd	−661	−0.00028	This study*
50166.37000		vis	−14 820	−0.01177	*	59503.78003	0.000099	ccd	−660.5	0.00076	This study*
50189.43470		vis	−14 785	−0.02761	*	59504.10892	0.000061	ccd	−660	−0.00007	This study*
50191.41290		vis	−14 782	−0.02774	*	59504.43961	0.00008	ccd	−659.5	0.00090	This study*
50193.39200		vis	−14 779	−0.02697	*	59504.76824	0.000029	ccd	−659	−0.00019	This study*
50432.11600		vis	−14 417	−0.02170	*	59505.09888	0.000081	ccd	−658.5	0.00073	This study*
50432.11600		V	−14 417	−0.02170	*	59505.42775	0.000015	ccd	−658	−0.00013	This study*
50502.02400		vis	−14 311	−0.01477	*	59505.75801	0.000076	ccd	−657.5	0.00041	This study*
50557.40700		vis	−14 227	−0.02507	*	59506.08720	0.000032	ccd	−657	−0.00012	This study*
50863.39500		vis	−13 763	−0.01909	*	59506.41753	0.000092	ccd	−656.5	0.00049	This study*
50871.30600		vis	−13 751	−0.02142	*	59506.74673	0.000058	ccd	−656	−0.00003	This study*
50898.35600		vis	−13 710	−0.00862	*	59507.07716	0.000109	ccd	−655.5	0.00067	This study*
51274.23200		ccd	−13 140	−0.01571	*	59507.40625	0.000082	ccd	−655	0.00004	This study*
51572.29890		vis	−12 688	−0.01750	*	59507.73660	0.000136	ccd	−654.5	0.00067	This study*
51650.77409	0.00007	ccd	−12 569	−0.01615	(11)	59508.06578	0.000108	ccd	−654	0.00013	This study*

https://doi.org/10.1017/pasa.2024.115 Published online by Cambridge University Press

Table B1. (Continued)

HJD (2400000+)	Error	Meth.	E	$O-C$ (d)	Ref.	HJD (2400000+)	Error	Meth.	E	$O-C$ (d)	Ref.
52297.02380		ccd	−11 589	−0.02157	*	59508.39595	0.000158	ccd	−653.5	0.00058	This study*
52585.86720		ccd	−11 151	−0.01465	(12)	59508.72526	0.000134	ccd	−653	0.00016	This study*
52606.31560		V	−11 120	−0.00902	*	59509.05550	0.000186	ccd	−652.5	0.00068	This study*
52628.73040	0.00020	ccd	−11 086	−0.01531	(13)	59509.38474	0.00016	ccd	−652	0.00020	This study*
52660.38300		V	−11 038	−0.01602	*	59509.71515	0.000213	ccd	−651.5	0.00089	This study*
52912.29320		V	−10 656	−0.01344	*	59510.04426	0.000184	ccd	−651	0.00028	This study*
52976.25740		V	−10 559	−0.01531	*	59510.37436	0.000245	ccd	−650.5	0.00065	This study*
53028.36400		vis	−10 480	−0.00478	*	59510.70373	0.000217	ccd	−650	0.00030	This study*
53055.39500		vis	−10 439	−0.01099	*	59511.03364	0.000272	ccd	−649.5	0.00049	This study*
53677.90920		V	−9 495	−0.01194	*	59511.36326	0.000237	ccd	−649	0.00039	This study*
53679.22860		V	−9 493	−0.01142	*	59513.67110	0.000419	ccd	−645.5	0.00017	This study*
53683.18500		V	−9 487	−0.01169	*	59514.00069	0.000354	ccd	−645	0.00004	This study*
53730.99780		V	−9 414.5	−0.00858	*	59514.33143	0.000417	ccd	−644.5	0.00106	This study*
53764.95700		vis	−9 363	−0.01075	*	59514.66020	0.000386	ccd	−644	0.00011	This study*
54085.44710	0.00200	−Ir	−8 877	−0.01044	(14)	59514.99077	0.000446	ccd	−643.5	0.00096	This study*
54126.33210	0.00100	−Ir	−8 815	−0.01097	(15)	59515.31970	0.000412	ccd	−643	0.00016	This study*
54127.65240	0.00030	ccd	−8 813	−0.00955	(16)	59515.65009	0.000458	ccd	−642.5	0.00083	This study*
54188.32170		ccdR	−8 721	−0.00910	*	59515.97921	0.000448	ccd	−642	0.00023	This study*
54505.51370	0.01300	V	−8 240	−0.00967	(17)	59516.30948	0.000483	ccd	−641.5	0.00078	This study*
54536.50650		V	−8 193	−0.01074	*	59516.63869	0.000471	ccd	−641	0.00027	This study*
54536.50680		R	−8 193	−0.01044	*	59517.29765	0.000477	ccd	−640	−0.00022	This study*
54536.50740		I	−8 193	−0.00984	*	59517.62777	0.000586	ccd	−639.5	0.00018	This study*
54552.33380		R	−8 169	−0.01010	*	59517.95713	0.000485	ccd	−639	−0.00018	This study*
54580.35640		V	−8 126.5	−0.01387	*	59518.28754	0.000618	ccd	−638.5	0.00051	This study*
54580.35900		R	−8 126.5	−0.01127	*	59518.61666	0.000507	ccd	−638	−0.00010	This study*
54580.35910		I	−8 126.5	−0.01117	*	59518.94707	0.000626	ccd	−637.5	0.00059	This study*
54824.02520	0.00010	R	−7 757	−0.00963	(18)	59519.27616	0.000545	ccd	−637	−0.00004	This study*
54857.32330		U	−7 706.5	−0.01345	(19)	59519.60639	0.000646	ccd	−636.5	0.00047	This study*
55207.16240		V	−7 176	−0.00940	*	59519.93567	0.00057	ccd	−636	0.00003	This study*
55255.96200		vis	−7 102	−0.00866	*	59520.26587	0.000689	ccd	−635.5	0.00050	This study*
55257.28010		I	−7 100	−0.00945	(20)	59520.59514	0.000587	ccd	−635	0.00005	This study*
55257.28014	0.00045	I	−7 100	−0.00941	(20)	59520.92545	0.000717	ccd	−634.5	0.00064	This study*
55472.91780		V	−6 773	−0.00994	*	59521.25466	0.000636	ccd	−634	0.00013	This study*
55507.20910		Rc	−6 721	−0.00973	*	59521.58489	0.000733	ccd	−633.5	0.00064	This study*
55534.24630		V	−6 680	−0.00973	*	59521.91415	0.000651	ccd	−633	0.00017	This study*
55542.15960		Rc	−6 668	−0.00976	*	59522.24433	0.000793	ccd	−632.5	0.00063	This study*
56698.49930	0.00690	−I	−4 914.5	−0.00514	(21)	59522.57365	0.000679	ccd	−632	0.00023	This study*
56706.40990	0.00580	−I	−4 902.5	−0.00787	(22)	59522.90371	0.0008	ccd	−631.5	0.00057	This study*
56714.32500	0.00960	−I	−4 890.5	−0.00609	(22)	59523.23306	0.000691	ccd	−631	0.00020	This study*
57080.31850	0.00400	−I	−4 335.5	−0.00402	(23)	59523.56325	0.000834	ccd	−630.5	0.00066	This study*
57826.48030		ccd	−3 204	−0.00312	*	59523.89262	0.000745	ccd	−630	0.00031	This study*
58564.40020		−Ir	−2 085	−0.00107	*	59524.22282	0.000854	ccd	−629.5	0.00079	This study*
58903.35400		ccd	−1 571	−0.00150	*	59525.87104	0.000785	ccd	−627	0.00040	This study*
59500.48289	0.00024	ccd	−665.5	0.00084	This study*	59526.20128	0.000962	ccd	−626.5	0.00092	This study*
59526.53063	0.000818	ccd	−626	0.00055	This study*	59549.94098	0.001818	ccd	−590.5	0.00063	This study*

https://doi.org/10.1017/pasa.2024.115 Published online by Cambridge University Press

Table B1. (Continued)

HJD (2400000+)	Error	Meth.	E	$O-C$ (d)	Ref.	HJD (2400000+)	Error	Meth.	E	$O-C$ (d)	Ref.
59526.86066	0.000963	ccd	−625.5	0.00085	This study*	59550.27026	0.001597	ccd	−590	0.00019	This study*
59527.18958	0.000873	ccd	−625	0.00005	This study*	59552.24877	0.00166	ccd	−587	0.00037	This study*
59527.51994	0.000991	ccd	−624.5	0.00069	This study*	59552.57865	0.001871	ccd	−586.5	0.00053	This study*
59527.84912	0.000912	ccd	−624	0.00015	This study*	59552.90821	0.001614	ccd	−586	0.00037	This study*
59528.17956	0.001032	ccd	−623.5	0.00087	This study*	59553.23788	0.001933	ccd	−585.5	0.00031	This study*
59528.50861	0.000928	ccd	−623	0.00019	This study*	59553.56777	0.001702	ccd	−585	0.00048	This study*
59528.83889	0.001161	ccd	−622.5	0.00075	This study*	59553.89737	0.001897	ccd	−584.5	0.00036	This study*
59529.16808	0.000967	ccd	−622	0.00022	This study*	59554.22714	0.001655	ccd	−584	0.00041	This study*
59529.49804	0.001122	ccd	−621.5	0.00046	This study*	59554.55713	0.001939	ccd	−583.5	0.00068	This study*
59529.82754	0.000992	ccd	−621	0.00024	This study*	59554.88639	0.001792	ccd	−583	0.00021	This study*
59530.15755	0.001099	ccd	−620.5	0.00052	This study*	59555.21622	0.001932	ccd	−582.5	0.00032	This study*
59530.48717	0.001021	ccd	−620	0.00042	This study*	59555.54581	0.001781	ccd	−582	0.00019	This study*
59530.81706	0.00113	ccd	−619.5	0.00059	This study*	59555.87547	0.001948	ccd	−581.5	0.00013	This study*
59531.14609	0.000991	ccd	−619	−0.00010	This study*	59556.20528	0.001856	ccd	−581	0.00022	This study*
59531.47616	0.001163	ccd	−618.5	0.00025	This study*	59556.53535	0.001913	ccd	−580.5	0.00056	This study*
59531.80541	0.001246	ccd	−618	−0.00023	This study*	59556.86477	0.001849	ccd	−580	0.00026	This study*
59532.13568	0.001182	ccd	−617.5	0.00032	This study*	59557.19467	0.002039	ccd	−579.5	0.00044	This study*
59532.46507	0.001042	ccd	−617	−0.00001	This study*	59557.52419	0.001881	ccd	−579	0.00024	This study*
59532.79536	0.001231	ccd	−616.5	0.00056	This study*	59557.85425	0.001967	ccd	−578.5	0.00058	This study*
59533.12455	0.001036	ccd	−616	0.00003	This study*	59558.18359	0.001882	ccd	−578	0.00019	This study*
59533.45503	0.001266	ccd	−615.5	0.00078	This study*	59558.51364	0.002059	ccd	−577.5	0.00052	This study*
59533.78409	0.001069	ccd	−615	0.00012	This study*	59558.84286	0.00182	ccd	−577	0.00002	This study*
59534.11404	0.001268	ccd	−614.5	0.00035	This study*	59559.17323	0.002032	ccd	−576.5	0.00067	This study*
59534.44353	0.001141	ccd	−614	0.00012	This study*	59559.50241	0.001818	ccd	−576	0.00012	This study*
59534.77367	0.001281	ccd	−613.5	0.00054	This study*	59559.83262	0.002095	ccd	−575.5	0.00061	This study*
59535.10299	0.001109	ccd	−613	0.00013	This study*	59560.16180	0.001885	ccd	−575	0.00007	This study*
59535.43315	0.00128	ccd	−612.5	0.00057	This study*	59560.49199	0.002118	ccd	−574.5	0.00054	This study*
59535.76253	0.001136	ccd	−612	0.00023	This study*	59560.82126	0.001813	ccd	−574	0.00009	This study*
59536.09258	0.00136	ccd	−611.5	0.00056	This study*	59561.15162	0.002143	ccd	−573.5	0.00073	This study*
59536.42203	0.001155	ccd	−611	0.00029	This study*	59561.48081	0.001922	ccd	−573	0.00018	This study*
59536.75183	0.001343	ccd	−610.5	0.00036	This study*	59561.81087	0.002127	ccd	−572.5	0.00053	This study*
59537.08147	0.001196	ccd	−610	0.00028	This study*	59562.14014	0.001908	ccd	−572	0.00008	This study*
59537.41123	0.001406	ccd	−609.5	0.00032	This study*	59562.47018	0.002176	ccd	−571.5	0.00040	This study*
59537.74091	0.001189	ccd	−609	0.00028	This study*	59562.79966	0.001946	ccd	−571	0.00016	This study*
59539.71948	0.001278	ccd	−606	0.00052	This study*	59563.12950	0.002208	ccd	−570.5	0.00027	This study*
59540.04950	0.001478	ccd	−605.5	0.00081	This study*	59563.45915	0.001891	ccd	−570	0.00020	This study*
59540.37885	0.00129	ccd	−605	0.00044	This study*	59563.78913	0.002147	ccd	−569.5	0.00046	This study*
59540.70854	0.001494	ccd	−604.5	0.00041	This study*	59564.11863	0.001968	ccd	−569	0.00024	This study*
59541.03793	0.001383	ccd	−604	0.00008	This study*	59564.44875	0.002158	ccd	−568.5	0.00064	This study*
59541.36808	0.001475	ccd	−603.5	0.00051	This study*	59566.09700	0.00199	ccd	−566	0.00028	This study*
59541.69741	0.001415	ccd	−603	0.00011	This study*	59566.42694	0.002196	ccd	−565.5	0.00049	This study*
59542.02741	0.001535	ccd	−602.5	0.00039	This study*	59567.08627	0.002275	ccd	−564.5	0.00037	This study*
59542.35689	0.001405	ccd	−602	0.00015	This study*	59567.41593	0.001956	ccd	−564	0.00031	This study*
59542.68699	0.001709	ccd	−601.5	0.00053	This study*	59567.74528	0.002265	ccd	−563.5	−0.00005	This study*
59543.01644	0.001439	ccd	−601	0.00026	This study*	59568.07533	0.001968	ccd	−563	0.00026	This study*

https://doi.org/10.1017/pasa.2024.115 Published online by Cambridge University Press

Table B1. (Continued)

HJD (2400000+)	Error	Meth.	E	$O-C$ (d)	Ref.	HJD (2400000+)	Error	Meth.	E	$O-C$ (d)	Ref.
59543.34655	0.001708	ccd	−600.5	0.00064	This study*	59568.40522	0.002283	ccd	−562.5	0.00044	This study*
59543.67591	0.001463	ccd	−600	0.00028	This study*	59568.73488	0.002024	ccd	−562	0.00038	This study*
59544.00573	0.001778	ccd	−599.5	0.00038	This study*	59569.06533	0.011441	ccd	−561.5	0.00111	This study*
59544.33535	0.001469	ccd	−599	0.00028	This study*	59569.39417	0.002078	ccd	−561	0.00022	This study*
59544.66530	0.001636	ccd	−598.5	0.00051	This study*	59569.72372	0.002489	ccd	−560.5	0.00005	This study*
59544.99450	0.001442	ccd	−598	−0.00002	This study*	59570.05363	0.002143	ccd	−560	0.00024	This study*
59545.32466	0.001668	ccd	−597.5	0.00042	This study*	59570.38360	0.002541	ccd	−559.5	0.00048	This study*
59545.65393	0.00141	ccd	−597	−0.00003	This study*	59570.71296	0.002098	ccd	−559	0.00013	This study*
59545.98409	0.001736	ccd	−596.5	0.00041	This study*	59571.04310	0.002568	ccd	−558.5	0.00055	This study*
59546.31335	0.001484	ccd	−596	−0.00005	This study*	59571.37254	0.00218	ccd	−558	0.00026	This study*
59546.64371	0.001716	ccd	−595.5	0.00058	This study*	59571.70230	0.002625	ccd	−557.5	0.00029	This study*
59546.97292	0.001476	ccd	−595	0.00007	This study*	59572.03196	0.00213	ccd	−557	0.00024	This study*
59547.30315	0.001726	ccd	−594.5	0.00058	This study*	59572.69140	0.002144	ccd	−556	0.00024	This study*
59547.63244	0.001548	ccd	−594	0.00015	This study*	59573.02137	0.003616	ccd	−555.5	0.00048	This study*
59547.96269	0.001771	ccd	−593.5	0.00068	This study*	59573.35084	0.00219	ccd	−555	0.00022	This study*
59548.29181	0.001556	ccd	−593	0.00007	This study*	59573.68097	0.004577	ccd	−554.5	0.00063	This study*
59548.62170	0.001843	ccd	−592.5	0.00024	This study*	59574.01034	0.002243	ccd	−554	0.00028	This study*
59548.95134	0.001591	ccd	−592	0.00016	This study*	59574.34014	0.002442	ccd	−553.5	0.00036	This study*
59549.28156	0.001767	ccd	−591.5	0.00066	This study*	59574.66954	0.002082	ccd	−553	0.00004	This study*
59549.61084	0.001583	ccd	−591	0.00022	This study*	59574.99978	0.002406	ccd	−552.5	0.00056	This study*
59575.32910	0.002032	ccd	−552	0.00015	This study*	59601.70697	0.002328	ccd	−512	0.00026	This study*
59575.65944	0.002404	ccd	−551.5	0.00077	This study*	59602.03660	0.00257	ccd	−511.5	0.00017	This study*
59575.98856	0.002125	ccd	−551	0.00018	This study*	59602.36645	0.002293	ccd	−511	0.00030	This study*
59576.31877	0.002441	ccd	−550.5	0.00065	This study*	59602.69592	0.002584	ccd	−510.5	0.00004	This study*
59576.64800	0.002104	ccd	−550	0.00017	This study*	59603.02591	0.002261	ccd	−510	0.00031	This study*
59576.97808	0.002448	ccd	−549.5	0.00053	This study*	59603.35574	0.00243	ccd	−509.5	0.00042	This study*
59577.30744	0.00211	ccd	−549	0.00017	This study*	59603.68532	0.00223	ccd	−509	0.00028	This study*
59577.63751	0.002371	ccd	−548.5	0.00051	This study*	59604.01500	0.002424	ccd	−508.5	0.00024	This study*
59577.96691	0.002178	ccd	−548	0.00019	This study*	59604.34466	0.00227	ccd	−508	0.00017	This study*
59578.29714	0.002414	ccd	−547.5	0.00069	This study*	59604.67462	0.002342	ccd	−507.5	0.00041	This study*
59578.62639	0.002165	ccd	−547	0.00023	This study*	59605.00414	0.002192	ccd	−507	0.00021	This study*
59579.94533	0.002116	ccd	−545	0.00027	This study*	59605.33409	0.002375	ccd	−506.5	0.00044	This study*
59580.27531	0.002465	ccd	−544.5	0.00053	This study*	59605.66353	0.002208	ccd	−506	0.00016	This study*
59580.60475	0.002202	ccd	−544	0.00025	This study*	59605.99364	0.002359	ccd	−505.5	0.00054	This study*
59580.93477	0.002494	ccd	−543.5	0.00056	This study*	59606.32296	0.00222	ccd	−505	0.00014	This study*
59581.26430	0.002211	ccd	−543	0.00036	This study*	59606.65312	0.002363	ccd	−504.5	0.00058	This study*
59581.59375	0.002375	ccd	−542.5	0.00009	This study*	59939.34204	0.00036	ccd	0	0.00000	This study
59581.92376	0.002134	ccd	−542	0.00038	This study*	59940.32978	0.00032	ccd	1.5	−0.00143	This study
59582.25341	0.002755	ccd	−541.5	0.00030	This study*	60237.08142	0.000092	ccd	451.5	0.00041	This study*
59582.58313	0.002247	ccd	−541	0.00031	This study*	60237.41168	0.000047	ccd	452	0.00094	This study*
59582.91302	0.002514	ccd	−540.5	0.00046	This study*	60237.74075	0.000088	ccd	452.5	0.00029	This study*
59583.24259	0.002283	ccd	−540	0.00031	This study*	60238.07101	0.000043	ccd	453	0.00083	This study*
59583.57202	0.002712	ccd	−539.5	0.00003	This study*	60238.40059	0.000087	ccd	453.5	0.00069	This study*
59583.90203	0.002149	ccd	−539	0.00031	This study*	60238.73032	0.000044	ccd	454	0.00069	This study*
59584.23141	0.002494	ccd	−538.5	−0.00003	This study*	60239.05990	0.000086	ccd	454.5	0.00055	This study*
59584.56138	0.002342	ccd	−538	0.00021	This study*	60239.38991	0.000044	ccd	455	0.00084	This study*

https://doi.org/10.1017/pasa.2024.115 Published online by Cambridge University Press

Table B1. (Continued)

HJD (2400000+)	Error	Meth.	E	$O-C$ (d)	Ref.	HJD (2400000+)	Error	Meth.	E	$O-C$ (d)	Ref.
59584.89110	0.0026	ccd	−537.5	0.00021	This study*	60239.71933	0.000091	ccd	455.5	0.00054	This study*
59585.22089	0.002262	ccd	−537	0.00029	This study*	60240.04940	0.000044	ccd	456	0.00089	This study*
59585.55050	0.002544	ccd	−536.5	0.00017	This study*	60240.37872	0.00009	ccd	456.5	0.00048	This study*
59585.88029	0.00229	ccd	−536	0.00024	This study*	60241.03822	0.00009	ccd	457.5	0.00054	This study*
59586.20963	0.003631	ccd	−535.5	−0.00015	This study*	60241.36824	0.000046	ccd	458	0.00084	This study*
59586.53969	0.002279	ccd	−535	0.00019	This study*	60241.69750	0.000091	ccd	458.5	0.00038	This study*
59586.86969	0.002952	ccd	−534.5	0.00047	This study*	60242.02779	0.000046	ccd	459	0.00094	This study*
59587.19913	0.002319	ccd	−534	0.00019	This study*	60242.35699	0.000088	ccd	459.5	0.00042	This study*
59587.52950	0.004687	ccd	−533.5	0.00084	This study*	60242.68712	0.000043	ccd	460	0.00083	This study*
59587.85866	0.002319	ccd	−533	0.00027	This study*	60243.01642	0.000087	ccd	460.5	0.00041	This study*
59588.18829	0.00446	ccd	−532.5	0.00018	This study*	60243.34663	0.000043	ccd	461	0.00090	This study*
59588.51807	0.002259	ccd	−532	0.00024	This study*	60243.67591	0.000092	ccd	461.5	0.00045	This study*
59588.84790	0.002924	ccd	−531.5	0.00035	This study*	60244.00610	0.000042	ccd	462	0.00092	This study*
59589.17754	0.002332	ccd	−531	0.00027	This study*	60244.33541	0.000091	ccd	462.5	0.00051	This study*
59589.50789	0.002568	ccd	−530.5	0.00089	This study*	60244.66552	0.000044	ccd	463	0.00090	This study*
59589.83692	0.002149	ccd	−530	0.00020	This study*	60244.99478	0.000088	ccd	463.5	0.00044	This study*
59590.16736	0.002557	ccd	−529.5	0.00092	This study*	60245.32505	0.000044	ccd	464	0.00098	This study*
59590.49636	0.002205	ccd	−529	0.00020	This study*	60245.65403	0.000092	ccd	464.5	0.00024	This study*
59590.82634	0.002564	ccd	−528.5	0.00046	This study*	60250.60053	0.00004	ccd	472	0.00091	This study*
59591.15589	0.00226	ccd	−528	0.00028	This study*	60250.92989	0.000085	ccd	472.5	0.00055	This study*
59591.48595	0.002626	ccd	−527.5	0.00062	This study*	60251.26004	0.000039	ccd	473	0.00098	This study*
59591.81535	0.002241	ccd	−527	0.00030	This study*	60251.58905	0.000088	ccd	473.5	0.00027	This study*
59592.14541	0.002574	ccd	−526.5	0.00064	This study*	60251.91951	0.000041	ccd	474	0.00100	This study*
59592.47468	0.002165	ccd	−526	0.00019	This study*	60252.24846	0.00008	ccd	474.5	0.00023	This study*
59592.80489	0.002609	ccd	−525.5	0.00067	This study*	60252.57902	0.00004	ccd	475	0.00107	This study*
59596.43148	0.00226	ccd	−520	0.00032	This study*	60252.90798	0.000088	ccd	475.5	0.00031	This study*
59596.76117	0.00273	ccd	−519.5	0.00029	This study*	60253.89777	0.000042	ccd	477	0.00093	This study*
59597.09092	0.00222	ccd	−519	0.00032	This study*	60254.22689	0.000091	ccd	477.5	0.00033	This study*
59597.42079	0.002541	ccd	−518.5	0.00047	This study*	60254.55714	0.00004	ccd	478	0.00086	This study*
59597.75031	0.002212	ccd	−518	0.00026	This study*	60254.88672	0.000092	ccd	478.5	0.00072	This study*
59598.07974	0.002579	ccd	−517.5	−0.00003	This study*	60255.21675	0.00004	ccd	479	0.00102	This study*
59598.40982	0.002203	ccd	−517	0.00033	This study*	60255.54609	0.00009	ccd	479.5	0.00064	This study*
59598.73946	0.00287	ccd	−516.5	0.00025	This study*	60255.87607	0.000039	ccd	480	0.00090	This study*
59599.06922	0.002262	ccd	−516	0.00029	This study*	60256.20532	0.000086	ccd	480.5	0.00043	This study*
59599.39933	0.009392	ccd	−515.5	0.00067	This study*	60256.53564	0.000039	ccd	481	0.00103	This study*
59599.72870	0.00222	ccd	−515	0.00032	This study*	60256.86454	0.00009	ccd	481.5	0.00020	This study*
59600.05827	0.006945	ccd	−514.5	0.00017	This study*	60257.19499	0.000037	ccd	482	0.00093	This study*
59600.71751	0.003389	ccd	−513.5	−0.00003	This study*	60257.52428	0.000088	ccd	482.5	0.00050	This study*
59601.04756	0.00225	ccd	−513	0.00029	This study*	60257.85448	0.000037	ccd	483	0.00098	This study*
59601.37709	0.002538	ccd	−512.5	0.00010	This study*	60258.18375	0.00009	ccd	483.5	0.00053	This study*
60258.51383	0.000039	ccd	484	0.00088	This study*	60277.30815	0.000081	ccd	512.5	0.00105	This study*
60264.77904	0.000092	ccd	493.5	0.00138	This study*	60277.63832	0.000046	ccd	513	0.00150	This study*
60265.10912	0.00004	ccd	494	0.00173	This study*	60277.96756	0.000088	ccd	513.5	0.00102	This study*
60265.43826	0.000079	ccd	494.5	0.00115	This study*	60278.29780	0.000041	ccd	514	0.00153	This study*
60266.09738	0.000081	ccd	495.5	0.00083	This study*	60278.62682	0.000093	ccd	514.5	0.00083	This study*

https://doi.org/10.1017/pasa.2024.115 Published online by Cambridge University Press

Table B1. (Continued)

HJD (2400000+)	Error	Meth.	E	$O-C$ (d)	Ref.	HJD (2400000+)	Error	Meth.	E	$O-C$ (d)	Ref.
60266.75699	0.000085	ccd	496.5	0.00099	This study*	60278.95735	0.000045	ccd	515	0.00164	This study*
60267.08733	0.000045	ccd	497	0.00161	This study*	60279.28609	0.000116	ccd	515.5	0.00066	This study*
60267.41645	0.000082	ccd	497.5	0.00101	This study*	60279.61666	0.000046	ccd	516	0.00151	This study*
60267.74675	0.000041	ccd	498	0.00159	This study*	60279.94584	0.000093	ccd	516.5	0.00096	This study*
60268.07561	0.000086	ccd	498.5	0.00073	This study*	60280.27618	0.000043	ccd	517	0.00158	This study*
60268.40617	0.00004	ccd	499	0.00157	This study*	60280.60518	0.000088	ccd	517.5	0.00086	This study*
60268.73500	0.000086	ccd	499.5	0.00067	This study*	60280.93565	0.000043	ccd	518	0.00161	This study*
60269.06576	0.000041	ccd	500	0.00171	This study*	60281.26469	0.000091	ccd	518.5	0.00093	This study*
60269.39478	0.000088	ccd	500.5	0.00101	This study*	60281.59498	0.000044	ccd	519	0.00150	This study*
60269.72507	0.000043	ccd	501	0.00158	This study*	60281.92419	0.000093	ccd	519.5	0.00098	This study*
60270.05414	0.00009	ccd	501.5	0.00092	This study*	60282.25444	0.000039	ccd	520	0.00151	This study*
60270.38447	0.000043	ccd	502	0.00153	This study*	60282.58357	0.00009	ccd	520.5	0.00092	This study*
60270.71360	0.000092	ccd	502.5	0.00094	This study*	60282.91403	0.00004	ccd	521	0.00166	This study*
60271.04410	0.000044	ccd	503	0.00172	This study*	60283.24304	0.000091	ccd	521.5	0.00095	This study*
60271.37303	0.00009	ccd	503.5	0.00093	This study*	60283.57336	0.000043	ccd	522	0.00154	This study*
60271.70353	0.000043	ccd	504	0.00171	This study*	60283.90237	0.000093	ccd	522.5	0.00083	This study*
60272.03277	0.000091	ccd	504.5	0.00122	This study*	60284.23275	0.000045	ccd	523	0.00149	This study*
60272.36284	0.000044	ccd	505	0.00157	This study*	60284.56200	0.000094	ccd	523.5	0.00102	This study*
60272.69203	0.000092	ccd	505.5	0.00104	This study*	60284.89227	0.000044	ccd	524	0.00156	This study*
60276.64867	0.000086	ccd	511.5	0.00101	This study*	60285.22132	0.000096	ccd	524.5	0.00089	This study*
60276.97904	0.000047	ccd	512	0.00166	This study*	60285.55172	0.000043	ccd	525	0.00157	This study*

Notes: '*':$O-C$ gateway; 'This study*':light minimums obtained by us based on the TESS light curves; (1) Rudiger (1983) (2) Kippenhahn (1953) (3) Diethelm et al. (1974) (4) Carnevali et al. (1975) (5) Agnesoni et al. (1978) (6) Locher (1979) (7) Agnesoni et al. (1980) (8) Diethelm et al. (1983a) (9) Diethelm et al. (1983b) (10) Andrakakou et al. (1983) (11) Nelson (2001) (12) Nelson (2003) (13) Dvorak (2003) (14) Hubscher (2007) (15) Hubscher et al. (2009) (16) Ogloza et al. (2008) (17) Hubscher et al. (2009) (18) Nelson (2009) (19) Brat et al. (2009) (20) Brat et al. (2011) (21) Hubscher (2014) (22) Hubscher & Lehmann (2015) (23) Hubscher (2016).

https://doi.org/10.1017/pasa.2024.115 Published online by Cambridge University Press

https://doi.org/10.1017/pasa.2024.115 Published online by Cambridge University Press

C. Physical parameters of the eclipsing binaries

Table C1. Physical parameters of the eclipsing binaries.

Name	Sp.type	Variable	Period	dp/dt	i	T_1	T_2	q	M_1	M_2	R_1	R_2	L_1	L_2	K_1	K_2	ref.	$v_1 \sin i$	$v_2 \sin i$
			(d)	(10^{-8} d yr^{-1})	(deg)	(K)	(K)		($M_\odot$)	($M_\odot$)	($R_\odot$)	($R_\odot$)	($L_\odot$)	($L_\odot$)	(km s^{-1})	(km s^{-1})		(km s^{-1})	(km s^{-1})
TYC6408-989-1	A4-	EB	0.470796		69.316	6 990	5 089	0.270	1.56	0.42	1.581	0.874	5.36	0.459			(1)	159	88
V2364 Cyg	kA4hA6mA7	EW	0.5921376	−16.2	81.6	7 310	6 542	0.319	1.8	0.55	2.11	1.23	11.35	2.48			(2)	178	104
GW Gem	kA4hF0mF0	EB/SD	0.7543173	**-2.41**	86.07	7 455	5 105	0.3666	1.72	0.64	2.29	1.48	24.43	1.93			This study	122	95
EU Peg	kA6hA8mA9	EA	0.721114	−7.33	81.3	8 730	5 064	0.3105	2.60	0.81	2.13	1.34	23.65	1.06			(3)	148	93
V404 Aur	kA2hA4mA6	EB	0.659444013	**+10.60**	81.11	8 483	5 496	0.3749	1.47	0.54	1.76	1.37	8.69	1.25			This study	130	84
V1073 Cyg	A3-F0	EW/KE	0.78585	−0.0104	69.85	7 300	6 609	0.303	1.810	0.549	2.545	1.481	9.77	3.01	66.45	219.09	(4)(5)(6)	154	90
FW Per	kA6hA8mA9	EA/SD:	0.7912215		89.9	6 900	5 060										(7)		
V2787 Ori	A4-F1	EB	0.810979		84.74	6 993	5 418	0.120	1.44	0.17	2.45	0.96	12.93	0.71			(8)	152	60
ES Cnc	kA7hF3mF3	EA/RS	1.067797	+0.051	68.3	7 325	5 975	0.777	1.94	1.50	2.05	1.47	10.8	2.5			(9)	90	65
XZ Per	kA6hF2mF1	EA/SD	1.15163412	−6.41	85.03	6 680	4 636	0.64	1.41	0.91	1.75	2.09	5.9	1.2			(10)(11)(12)	77	91
XZ UMa	kA5hA8mF0	EA/SD	1.2223042	−0.0133	83.96	7 766	5 346	0.626	1.92	1.2	1.70	2.38	9.5	4.2			(13)(14)	70	98
CO Cam	A4-F3	EB	1.27095		48.9	7 080	5 050	0.58	1.48	0.86	1.83	0.84			72.3	124	(15)	55	25
DV Aqr	A4-F0	EB	1.575529		70	7 905	6 056	0.6	2	1.2	3	2					(16)(17)	91	60
CM Lac	A2-A4	EA/DM	1.604691434		86.9	8 700	7 034	0.76	1.98	1.50	1.51	1.55	11.8	5.3	119	156	(18)	48	49
HO Tel	A2-A7	EA	1.613101		81.01	7 872	7 627	0.921	1.88	1.73	2.28	2.08	17.96	13.17	131.45	142.75	(19)	71	64
RW Leo	kA1hA2mA3	EA/SD	1.6825565	17.8													(20)(21)		
V0885 Cyg	A2-	EB/DM	1.694795		70.64	8 375	8 150	1.144	2.005	2.234	2.345	3.385	23.988	45.709	143.58	128.86	(22)	66	95
V1637 Ori	kA3hA7mA8	EA	1.82276		77.61	8 500	5 296	0.555	2.1	1.166	2.22	3.12	23	6.85			(23)	60	85
V2083 Cyg	A3-A9	EA	1.867493429		80.47	7 630	7 623	0.97	1.71	1.66	2.12	2.45					(24)	57	65
TX Her	A5-A9	EA/DM	2.0598094	+49.3	88.3	8 180	7 536	0.895	1.61	1.44	1.53	1.51	9.44	6.56			(25)	38	37
V0397 Cep	A2-	EA	2.086835			9 730	9 588	0.9824									(26)		
RV Lyn	kA5hA9mF0	EA/SD	2.30751		84.91	6 700	4 287	0.69									(27)		
V0477 Cyg	A1-A3	EA/DM	2.3469906		85.66	8 730	6 531	0.749	1.80	1.35	1.60	1.42	13.183	3.311			(28)	34	31
WW Aur	A2-A8	EA/DM	2.52501922		87.55	8 000	7 637	0.9227	1.964	1.814	1.927	1.841	13.459	10.533	116.81	126.49	(29)	39	37
EE Peg	A2-A5	EA/DM	2.62821423		88.6	8 531	6 324		2.01	1.29	2.02	1.27	19.498	2.291	89.5	140.2	(30)(31)	39	24
TX Ari	kA1hA2mA3	EA	2.691352		80.4	9 200	4 400	0.31	2.21	0.69	2.55	3.61					(32)	47	67
XY Cet	A1-F0	EA/DM	2.780714		87.66	7 870	7 620	0.9108	1.773	1.615	1.873	1.773	12.078	9.506	108.3	118.9	(33)	34	32
CF Tuc	F -	EA/RS	2.7975	−4.9	69.91	6 100	4 286	1.117	1.11	1.23	1.63	3.60	3.32	3.91	98.92	88.55	(34)(35)	28	61
TW Dra	A6-F1	EA/SD	2.806847	+339	86.8	8 160	4 538	0.411	2.2	0.90	2.58				64.05	150	(36)(37)(38)	46	

Table C1. (Continued)

Name	Sp.type	Variable	Period (d)	dp/dt (10^{-8} d yr^{-1})	i (deg)	T_1 (K)	T_2 (K)	q	M_1 ($M_\odot$)	M_2 ($M_\odot$)	R_1 ($R_\odot$)	R_2 ($R_\odot$)	L_1 ($L_\odot$)	L_2 ($L_\odot$)	K_1 (km s^{-1})	K_2 (km s^{-1})	ref.	$v_1 \sin i$ (km s^{-1})	$v_2 \sin i$ (km s^{-1})
BW Boo	A0-A4	EA/DM	3.332816		81.4	8 900	5 250	0.56	2.0	1.1	1.9	1.2	21.62	1.24	74.2	134	(39)	29	18
DV Boo	A2-	EA	3.782634		82.995	7 400	6 398	0.7457	1.629	1.215	1.966	1.286	10.471	2.500	82.08	110.08	(40)	26	17
V0624 Her	A3-A9	EA/DM	3.894977			8 147	7 943	0.8238	2.27	1.87	3.03	2.21	36.308	16.982	96.6	117.2	(41)(42)		
YY Boo	kA7hF0mF1	EA/SD+DSCT	3.933049			81.7	4 650	0.29									(43)		
bet Aur	A1-A3	EA/DM	3.960036			9 350	9 200	0.964	2.376	2.291	2.762	2.568			107.75	111.25	(44)		
MY Cyg	A5-F2	EA/DM	4.0051873		88.58	7 100	7 036	0.994	1.82	1.80	2.22	2.28	11.220	11.482	102.4	103.0	(45)	28	29
AR Aur	AmFm	EA/DM	4.134651			10 950	10 350	1	2.48	2.29	1.78	1.82			114	114	(46)(47)		
GV Car	A0-	EA/DM	4.294621			10 100	7 750		2.51	1.54	2.57	1.43					(48)		
YZ Cas	A2-A4	EA/DM	4.467222		88.332	9 520	6 880	0.585	2.263	1.325	2.525	1.331	46.989	3.565	73.05	124.78	(49)(44)	29	15
GZ CMa	A0-	EA/DM	4.80085		86.8	8 810	8 531	0.909	2.20	2.00	2.49	2.13	33.497	21.627	96.8	106.5	(50)	26	22
V0788 Cen	A2-F2	EA/D	4.966377		82.821	7 820	7 405	0.7881	1.9621	1.5463	2.733	1.642	25.2	7.31	82.918	105.21	(51)	28	17
HD 55822	A3-F5	EA	5.1229			7 300			1.65		2.0				40.20		(52)		
V1260 Tau	A3-	EA	5.430835		86.98	7 500	7 557	1.11			2.11	2.81					(53)(54)	20	26
V0396 Gem	kA3mA4	EA	5.4966		83.27	7 000	6 978	0.990	1.814	1.797	2.655	2.659	15.276	15.136	91.46	92.36	(55)	24	24
S Vel	A4-A8	EA/SD	5.9336475			8 453	4 074	0.17	1.8	0.3	1.5	4.2	10.28	4.355			(56)		
V0364 Lac	A1-A8	EA/DM	7.351522		89.19	8 250	8 500	0.9838	2.333	2.296	3.307	2.985	45.394	41.687	94.47	96.02	(57)	23	21
KW Hya	A1-A9	EA/DM	7.7499942		87.65	8 000	6 881	0.753	1.978	1.488	2.126	1.484	16.596	4.467	70.14	93.20	(58)(59)	14	10
EI Cep	A7-F2	EA/DM	8.43935	−301	87.23	6 750	6 950	1.0544	1.7716	1.6801	2.896	2.329	31.117	11.350	76.84	81.03	(60)	17	14
RR Lyn	A3-F1	EA/DM	9.945079		87.46	7 770	7 180	0.7790	1.9394	1.5100	2.564	1.613	21.577	6.237	65.65	83.92	(61)(62)	13	8
V4090 Sgr	A2-F1	EA/DM	11.41507		87.4	7 700	5 800	0.5163	2.15	1.11	1.95	0.91	13.489	0.955	47.7	92	(63)	9	4
RX Gem	kA2hA5mA9	EA/DS	12.2086588		81.51	9 450	4 405	0.145	2.96	0.429	3.36	7.66	7.82	4.864	157	119.9	(64)(65)	14	31
EY Ori	A7-F4	EA/D	16.787832		88.9	7 760	5 940	0.5714	3.5	2	5.6	3.5			150		(66)(67)	17	11
MP Del	A3-	EA	21.3387		88.14	7400	6927	0.8004	1.559	1.248	2.428	1.575	15.9	5.26	48.72	60.87	(68)	6	4
PQ Vel	A2-	EA	22.2632		89.9	9000	7100	0.5536	2.8	1.55	4.35	1.55	111	6			(69)	10	4
RZ Eri	A5-	EA/DS/RS	39.28238		89.61	7400	4670	0.963	1.69	1.63	2.84	6.94	21.380	20.417	50.8	48.9	(70)(71)	4	9

Notes: (1) Tian (2021) (2) Yuan et al. (2020) (3) Yang et al. (2018) (4) Pribulla et al. (2006) (5) Ekmekçi et al. (2012) (6) Tian et al. (2018) (7) Zasche (2015) (8) Tian et al. (2019) (9) Yakut et al. (2009) (10) Qian (2001) (11) Michaels (2017) (12) Khaliullina (2021) (13) Nelson et al. (2006) (14) Soydugan et al. (2011) (15) Kurtz et al. (2020) (16) Okazaki et al. (1985) (17) Polubek (2001) (18) Liakos & Niarchos (2012) (19) Sürgit et al. (2017) (20)Qian (2003) (21) Liao & Qian (2010) (22) Lacy et al. (2004) (23) Ulaş et al. (2022) (24)Zasche et al. (2012) (25) Zhu et al. (2019) (26) Bulut et al. (2005) (27) Zasche (2017) (28) Değirmenci et al. (2003) (29) Southworth et al. (2005) (30) Linnell et al. (1995) (31) Popper (1981) (32) Bakış et al.Bak (2022) (33) Southworth et al. (2011) (34) Doğru et al. (2009) (35) Jableka et al. (2012) (36)Tkachenko et al. (2010) (37) Liao et al. (2016) (38) Chaplin (2019) (39) Glazunova (2011) (40) Kahraman Aliçavuş & Aliçavuş (2020) (41) Popper (1984) (42) Zasche et al. (2020) (43) Hambsch et al. (2010) (44) Takeda et al. (2019) (45) Tucker et al. (2009) (46) Rachkovskaia (1985) (47) Zverko et al. (1997) (48) Southworth & Clausen (2006) (49) Pavlovski et al. (2014) (50) Popper et al. (1985) (51) Graczyk et al. (2022) (52) Carquillat et al. (2003) (53) Smalley et al. (2014) (54) Bulut (2022) (55) Yücel & BakışYücel & Bak (2022) (56) Garc a et al. (1990) (57) Torres et al. (1999) (58) Andersen & Vaz (1984) (59) Gallenne et al. (2019) (60) Torres et al. (2000) (61) Khaliullin & Khaliullina (2002) (62) Southworth (2021) (63) Gallenne et al. (2019) (64) Glazunova et al. (2008) (65) Olson & Etzel (2015) (66) Ismailov (1987) (67) Zakirov (1998) (68) Ibanoğlu et al. (2008) (69) Hauck (2011) (70) Popper (1988) (71) Vivekananda Rao et al. (1994).